Insect Systematics and Diversity, 2026, **10**(5), ixag040
DOI: https://doi.org/10.1093/isd/ixag040
Research

ENTOMOLOGICAL SOCIETY OF AMERICA
SHARING INSECT SCIENCE GLOBALLY

OXFORD

Evolution

Phylogeography of *Bombus huntii* (Hymenoptera: Apidae) using whole-genome sequences from natural history collection specimens

Brandon A. Meadows*[,1], Jonathan B. Uhuad Koch[2], Rémy Vandame[3], Michael G. Branstetter[4], Ava G. McKallip[1], and Jeffrey D. Lozier*[,1]

[1]Department of Biological Sciences, The University of Alabama, Tuscaloosa, AL, USA
[2]Pacific Cooperative Studies Unit, College of Natural Sciences, University of Hawai'i at Mānoa, Honolulu, HI, USA
[3]El Colegio de la Frontera Sur (ECOSUR), Departamento Agricultura Sociedad y Ambiente, San Cristóbal de Las Casas, Chiapas, Mexico
[4]United States Department of Agriculture, Agricultural Research Service, Pollinating Insects Research Unit, Utah State University, Logan, UT, USA

*Corresponding authors. Brandon A. Meadows, Department of Biological Sciences, The University of Alabama, Box 870344, Tuscaloosa, AL 35487, USA (Email: bameadows2@crimson.ua.edu); Jeffrey D. Lozier, Department of Biological Sciences, The University of Alabama, Box 870344, Tuscaloosa, AL 35487, USA (Email: jlozier@ua.edu).

Subject Editor: Heather Hines

Bumble bees are widespread pollinators, and species often span heterogeneous landscapes with varying environmental complexity. Complex topography, along with historical climate, can shape genetic diversity and act as barriers to gene flow, potentially leading to speciation. *Bombus huntii* (Greene, 1860) is a bumble bee species featuring a broad geographic range, spanning from the southern portion of Canada, the western United States, to the central portion of Mexico. Prior microsatellite work identified signatures of population structure between the northern portion of *B. huntii*'s range, in the United States and Canada, and the northern and central portions in Mexico. Utilizing a newly assembled reference genome and whole-genome resequencing of natural history collection specimens, we aimed to characterize patterns of population structure, genetic diversity, and inbreeding for northern and southern populations of *B. huntii* and test for potential speciation based on prior microsatellite results. We found strong population structure between the northern and southern lineages and identified reduced genetic diversity in the southern populations with evidence of increased inbreeding compared to the north. Our phylogenomic results lacked strong support for splitting the north and south populations into separate species, with demographic analysis suggesting some gene flow in the direction of south to north. Overall, our results suggest that while there is a lack of strong support for speciation occurring between these 2 geographic populations, there is evidence of decreased genetic diversity and increased levels of inbreeding in the Mexico population, indicating that these 2 populations do warrant consideration as evolutionary significant units.

Keywords: Bombus, genomics, museomics, phylogenomics

Introduction

Bumble bees (Hymenoptera: Apidae: *Bombus* Latreille, 1802) are important pollinators in both agricultural and wildland settings (Velthuis and Van Doorn 2006, Button and Elle 2014). Bumble bee species often have broad geographic ranges that span heterogeneous landscapes, and for taxa that inhabit montane areas, such landscape complexity can impose barriers to gene flow between populations and potentially drive speciation (Jha 2015, Jackson et al. 2018, Ghisbain et al. 2020, Glück et al. 2022, Sousa et al. 2023). In part due to such large geographic ranges, species delimitation has historically been difficult in bumble bees, and taxonomic uncertainty has been widespread across the genus (Williams 1998, Duennes et al. 2017). Molecular data has facilitated investigation of species status in bumble bees by assisting with identification of evolutionary independent lineages (De Queiroz 2007, Williams 2022, Williams et al. 2022), and several recent genetic studies within bumble bees have helped clarify existing taxonomy or identify intraspecific lineages that could be elevated to species (Williams et al. 2016, Ghisbain et al. 2020, Williams 2021, Beckham et al. 2024). Even in the absence of species divergence, investigating population dynamics can be fruitful for

Received: 10 April 2026. **Revised:** 30 July 2026. **Accepted:** 20 August 2026

uncovering genetically isolated populations and varying levels of genetic diversity across species ranges. The shift from small numbers of genetic markers to genome-scale data has improved the ability to reveal historical demographic patterns (Lozier 2014, Zimmerman et al. 2020, Lozier et al. 2023, Sang et al. 2024). Genome-wide investigation of bumble bees near the species level is becoming increasingly important for biological conservation of imperiled species and commercial development of native species for agricultural pollination (Baur et al. 2019, Cruz et al. 2024). Specifically, these data have improved the capacity to identify cryptic species, evolutionary significant units, and reduced levels of genetic variation (Cameron and Sadd 2020, Ghisbain et al. 2020).

Bombus huntii Greene, 1860 is a widespread bumble bee found throughout western North America, ranging from southern British Columbia in Canada to the north, to the Trans-Mexican Volcanic Belt in the south (Koch et al. 2012). *Bombus huntii* is an effective agricultural pollinator due to its native abundance, capacity for captive rearing, and its effective pollination of obligate buzz-pollination crops such as tomatoes (Strange 2015, Baur et al. 2019) and is now a managed native pollinator in western North America (Strange et al. 2023). Growing recognition of this species' economic importance highlights the value of more genetic and genomic data to better assess population health, ecological traits, and evolutionary lineages. Such information can improve our understanding of *B. huntii* as a North American pollinator and guide efforts to preserve regional genetic diversity. Understanding regional signatures of population structure and genetic diversity is especially important when it comes to commercial pollination. Movement of commercial pollinator species into regions with differing genetic backgrounds poses the risk of eroding unique genetic variation present in the native population (e.g. outbreeding depression) as well as the possibility of the commercial pollinators outcompeting the native population for local resources. Therefore, gaining a comprehensive understanding of *B. huntii* population structure and genetic diversity is essential for mitigating potential risks as the commercial use of *B. huntii* as a pollinator continues to expand.

A previous microsatellite study of *B. huntii* investigated population structure and diversity across the United States (US), Canada, and Mexico, and identified strong population structure between samples comprising populations primarily in the US and Canada with those from Mexico (Koch et al. 2018). This study also identified important effects from Pleistocene climate dynamics, with populations of *B. huntii* in regions that have been more climatically unstable during the Pleistocene, corresponding to higher latitudes in the northern part of *B. huntii*'s range, actually featuring greater levels of genetic diversity compared to *B. huntii* populations in the south, where the climate has been more stable during the last glacial-interglacial period. The contemporary distribution of climatically suitable habitat provides a hypothesis for the observed patterns of population structure (Fig. 1), with more northern portions of *B. huntii's* range featuring large continuous regions of suitable habitat, while *B. huntii* in Mexico occupies a much more fragmented montane landscape where it largely occurs at higher elevations. Thus, in the north, *B. huntii* likely has the potential for widespread gene flow, while southern populations may have limited dispersal with the northern populations and each other, resulting in reduced genetic connectivity and diversity. The strong population structure identified in Koch et al. (2018), combined with recent discovery (or rediscovery) of other bumble bee species using molecular data (e.g. *B. vancouverensis*/*B. bifarius*, *B. occidentalis*/*B. mckayi*) (Sheffield et al. 2016, Ghisbain et al. 2020, Williams 2021, Rohde et al. 2025), has raised some interest in testing the species status of *B. huntii* populations and whether these populations may harbor evolutionarily distinct genomic variation. The recent publication of a reference genome for *B. huntii* enables an examination of this possibility using genome-wide data to test the species status of *B. huntii* (Koch et al. 2024), similar to recent assessments in other bumble bees (Ghisbain et al. 2020, Rohde et al. 2025).

With some bumble bee species declining, developing low-harm sampling approaches that reduce the need to sacrifice bees for collecting genetic data will become an increasingly attractive avenue for researchers. The availability of bumble bees in natural history collections has the potential to open the door for genomic studies that minimize the need for new sampling from potentially sensitive natural populations (Yeates et al. 2016, Card et al. 2021). Modern shotgun library preparation methods allow whole-genome resequencing from small amounts of DNA from museum specimens, and the large amount of genetic data from whole genomes allows for robust inferences even from relatively few samples (Sproul and Maddison 2017, Schweizer et al. 2025). In this study, we use specimens housed in natural history collections for whole-genome resequencing of *B. huntii* throughout its geographic range to examine the effectiveness of bumble bee "museomics" to pursue phylogenomic and population genomic analyses. We test the hypothesis that the *B. huntii* found in Mexico could be recognized as a unique species (independent evolutionary lineage) from the samples found in the United Stataes and Canada, or if the species may otherwise harbor unique patterns of genetic diversity that warrant consideration as an evolutionary significant unit. To achieve this goal, we characterize genome-wide population genetic signatures including population structure and genetic diversity at multiple scales (locality, individual, and genome). Furthermore, to test our speciation hypothesis, we employed multiple phylogenetic tools and performed demographic reconstruction.

Methods

Samples

Samples used in this study were from pinned natural history collection specimens collected between 2004 and 2015 from across the *B. huntii* range (average age = 10 ± 1 SE years old). Specimens from the United States and Canada were obtained from the US National Pollinating Insects Collection (BBSL) at the USDA ARS Pollinating Insects Research Unit (PIRU) in Logan, UT, US. Single mid-leg tissues for specimens from Mexico were obtained from the El Colegio de la Frontera Sur (ECOAB-ECOSUR) collection. The specimens were collected between 2012 and 2014 in a bumblebee nationwide survey funded by a CONABIO (National Commission for the Knowledge and Use of Biodiversity) grant JE016. In total, we include data from 37 diploid female workers with successfully resequenced whole genomes from 13 unique states/provinces, henceforth referred to as sampling localities ($n = 1$ from Canada, $n = 9$ from the United States, $n = 3$ from Mexico) (Fig. 1). DNA was extracted from homogenized whole specimens for BBSL samples using the Zymo Quick-DNA Miniprep Plus kit (Zymo

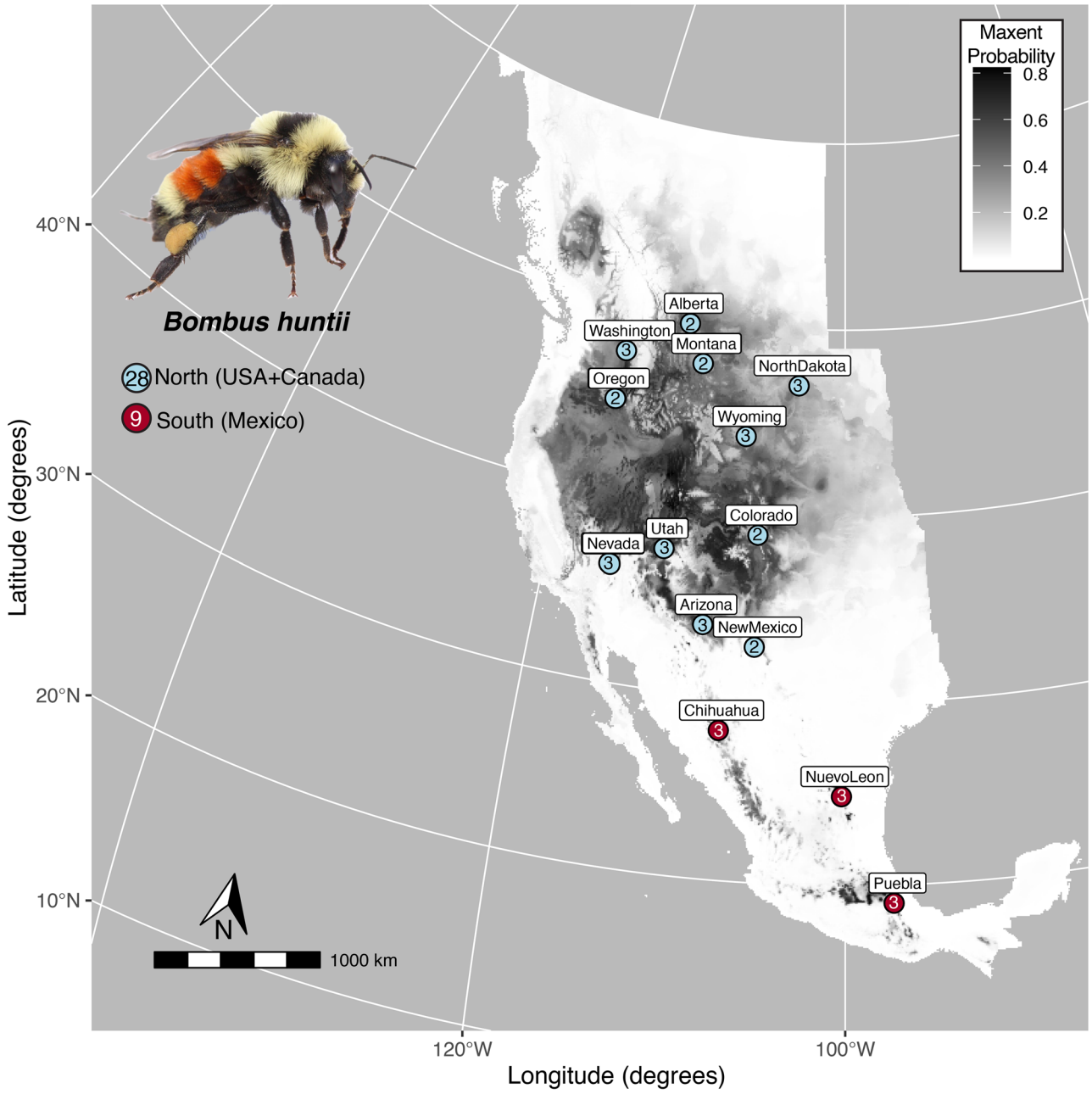

Fig. 1. Map of sampling localities with colors of the points indicating geographic origin (numbers indicate final sample sizes). The shading of the map represents habitat suitability as determined by Maxent probability. Darker shades indicate greater habitat suitability compared to lighter shades.

Research) or single mid-legs for Mexican samples using the Qiagen DNeasy Animal Tissues protocol (Qiagen Sciences, Germantown, MD, USA). Isolated DNA for each sample was subjected to a standard 0.9× Ampure XP magnetic bead purification (Beckman Coulter, Brea, CA, USA) to remove small DNA fragments and concentrate DNA. The resulting DNA was quantified by Qubit HS DNA fluorometry and visualized on an agarose gel before proceeding to library preparation for sequencing. In addition to *B. huntii* we also obtained whole genome data from several outgroups representing the most closely related species from the clade containing *B. huntii* within the *Bombus* subgenus *Pyrobombus* (Hines et al. 2006), including 2 diploid samples each from *B. impatiens* (IN08.0492 and AL09.0353 collected by Cameron et al. 2011, processed and sequenced for this study), *B. bifarius* (CO08.0108 and CO08.0606 collected by Cameron et al. 2011, processed and sequenced for this study), *B. vancouverensis* (previously published in Heraghty et al. [2022]; JDL1289, SRA accession SRX16239261 and JDL1539, SRA accession: SRX16239324), and *B. vosnesenskii* (previously published in Heraghty et al. [2023]; JDL1146, SRA accession SRX18700522 and JDL3158, SRA accession SRX18700514).

DNA Barcoding

We conducted PCR amplification of a fragment of the cytochrome oxidase I gene (COI) on 29 samples as an initial evaluation of possible species status in *B. huntii* lineages. The COI gene, or "barcoding gene," is regularly used to differentiate

diverse insect taxa at the species level (e.g. Hebert et al. 2003, Carolan et al. 2012). PCR was performed using the oligonucleotide primers LCO1490 and HCO2198 (Folmer et al. 1994), largely as previously described (e.g. Lozier et al. 2020), in 25 µl reactions with the GoTaq Flexi polymerase system (Promega, Madison, WI, USA; 1 µl DNA isolate; 5 µl 5× buffer; 2.5 µl MgCl2 at 25 mM; 1 µl each primer at 10 µM concentration; 0.5 µl dNTP at 10 mM each; 13.75 µl sterile H_2O; 0.25 U GoTaq polymerase). Thermocycling conditions for this reaction were: 95 °C for 5 min; 33 cycles of 95 °C for 30 s, 49 °C for 45 s, and 72 °C for 45 s; 72 °C for 5 min; 12 °C hold. After confirmation of amplification success with gel electrophoresis, products were cleaned with ExoSAP-IT (Applied Biosystems, USA) and sequenced in both directions by Sanger sequencing at Eurofins Genomics (Louisville, KY, USA). Geneious Prime version 2022.2.2 (BioMatters, Ltd, Auckland, New Zealand) was used for all sequence inspection, editing, assembly, and alignment. Individual forward and reverse sequences were assembled for each sample using the *de novo* assembly function in Geneious and quality-trimmed by removing any base pair with greater than a 1% chance of error and manually checked for other errors. Sequences were compiled into a consensus sequence and aligned using the Geneious aligner, and ragged ends of the alignment were trimmed to 516 base pairs (bp) total length per sample. Sequences have been submitted to NCBI GenBank (Accessions: PP646191-PP646219). In addition to the 29 new samples sequenced, we added sequences from 17 samples that had previously been uploaded to GenBank to better represent the *B. huntii* range, including Canada. To visualize COI sequence variation and regional relationships, we generated a TCS haplotype network (Clement et al. 2000) using the software PopArt v1.7 (Leigh and Bryant 2015). A mapping file was used to denote sample regional origin as Canada, United States, or Mexico, which was selected as a sufficient resolution for visualization after viewing the level of sequence variation (see Results). The TCS network was generated using PopArt's default settings. A table with sequences, GenBank accession numbers, and sample metadata is provided as a data supplement (Supplementary Data File S1).

Whole-Genome Sequencing and Bioinformatics

Whole-genome sequencing libraries were prepared following the manufacturer's instructions using the NEB Ultra II FS DNA Library Prep Kit (New England BioLabs, Ipswich, MA, USA) with 8 bp dual-indexing using NEB Multiplex Oligos for Illumina. Libraries were quantified by Qubit HS fluorometry and diluted and pooled using the Illumina Pooling Calculator (support.illumina.com/help/pooling-calculator/pooling-calculator.htm). The multiplexed library was sequenced (150 bp paired-end) on ~1/4 of an Illumina NovaSeq 6000 lane at Psomagen Inc (Rockville, MD, USA) to a mean of 5.33×10^9 (1.63×10^9 SD) bp from 3.53×10^7 (1.08×10^7 SD) reads per sample. Paired end FASTQ files have been submitted to the NCBI Sequence Read Archive (BioProject PRJNA1167783). FASTQ files were processed to remove adapters and trim poor quality bases and reads using the Trim Galore! wrapper (https://github.com/FelixKrueger/TrimGalore) for CutAdapt and FastQC (Martin 2011, Wingett and Andrews 2018), using default settings except using the 2-color base quality cutoff mode (--2colour 20) as recommended for the NovaSeq platform to avoid G-overcalling at low-quality bases.

We used bwa mem version 0.7.15-r1140 (Li 2013) to align the trimmed reads to the *B. huntii* reference genome assembly (NCBI Refseq ID: GCF_024542735.1). We then used Samtools v1.10 (Li et al. 2009) to convert the SAM files into BAM files and Picard version 2.23.9 (http://broadinstitute.github.io/picard/) to sort and index the bam files and mark duplicate reads. We called single nucleotide polymorphisms (SNPs) using GATK version 4.4.0.0 (McKenna et al. 2010) in 3 steps. First, we used the command HaplotypeCaller to produce GVCF files per individual, then used GenomicsDBImport to import the GVCFs into GenomicsDBs, and finally used GenotypeGVCFs, with the command—include-non-variant-sites to retain the invariant sites, on each GenomicsDB workspace to obtain VCFs for each of the 18 main scaffolds that represent the 18 *B. huntii* chromosomes (NCBI RefSeq Accessions NC_066238.1—NC_066255.1). Chromosomal VCFs were merged using BCFTools v1.21 (Danecek et al. 2021).

Population Genetics Analyses

SNP Dataset Filtering

We used VCFTools v0.1.15 (Danecek et al. 2011) to filter the raw GATK output VCF (invariant + variant sites) for use in genome-wide analyses. The raw GATK output VCF contained 279,265,701 sites with 10,214,273 SNPs and a mean depth of coverage of 12.4× (Table 1). For population genetics analyses of heterozygosity and population structure we first removed the outgroup individuals listed above. Next, we filtered the raw VCF to retain the variant + invariant sites ("all sites" dataset) with the following parameters: --max-missing 0.70—minDP 6—max-meanDP 40—max-alleles 2—remove-indels; we used depth filters here because invariant sites do not possess quality scores (Table 1). We then used VCFtools to produce 3 SNP-only datasets from the raw GATK output VCF file: a "full" dataset, a "high depth" dataset, and a "low missing data" dataset to evaluate different filtering criteria on results. The full dataset retained a larger set of SNPs but allowed for more missing data and did not apply a thinning filter, the high depth dataset contained the same filtering parameters as the full dataset with the exception of a stringent minimum depth filter, and the low missing data dataset allowed for at most 2 missing genotypes per SNP (96% complete data) and only retained one SNP per kb. For the "full" SNP dataset, we used VCFtools to perform an initial round of filtering with the following parameters: --max-missing 0.70—minGQ 20—minQ 30—min-alleles 2—max-alleles 2—remove-indels followed by a minor allele frequency (maf) filter of 0.05 to remove low-frequency variants, resulting in 1,172,743 SNPs at ≥0.05 minor allele frequency, <30% missing data and a mean depth of coverage of 12.9× (Table 1). Finally, for the "high depth" SNP dataset and the "low missing data" SNP dataset, we used the same parameters as described above except we applied a –minDP filter of 15 to the "high depth" dataset and we used a—max-missing filter of 0.96 (allowing at most 2 missing samples for a genotype) and a—thin filter of 1,000 bp for the "low missing data" dataset (Table 1).

We tested for relatedness (using the low missing data file) following the approach in Jackson et al. (2018) with the relatedness2 function of VCFtools and only identified one pair of bees from the Arizona population to be likely colony-mates (BBSL754228 and BBSL754238). Given the limited evidence for widespread sib-level relatedness and the impact of this

Table 1. Summary of SNP datasets filtered using VCFtools

Analysis	Individuals	SNP filtering criteria	Analyses performed	Total records
Starting dataset—Raw GATK output (variant and invariant) with outgroups	28 North, 9 South, outgroups	None, raw GATK output, includes variant and invariant sites	None	279,265,701 total sites; 10,214,273 SNPs
***B. huntii* "All Sites" dataset**	28 North, 9 South	30% missing data, minimum depth 6, maximum mean depth 40×, max alleles = 2, indels removed (depth filters employed in absence of genotype qualities for invariant sites)	Pixy	220,914,228 total sites; 8,825,048 SNPs
***B. huntii* "Full" dataset**	28 North, 9 South	Q = 30, GQ = 20, 30% missing data, biallelic, indels removed, maf = 0.05	sNMF, PCA, F_{ST}, heterozygosity, ROH	1,172,743 SNPs
***B. huntii* "Low Missing Data" dataset**	28 North, 9 South	Q = 30, GQ = 20, 4% missing data (2 missing genotypes per SNP), biallelic, indels removed, maf = 0.05, thin = 1,000	sNMF, pca, F_{ST}, heterozygosity	27,500 SNPs
***B. huntii* "High Depth" dataset**	28 North, 9 South	Q = 30, GQ = 20, 30% missing data, biallelic, indels removed, maf = 0.05, minimum depth = 15	Heterozygosity	5,541 SNPs
IQ-TREE dataset	28 North, 9 South, outgroups	Q = 30, GQ = 20, biallelic, 20% missing, 1 SNP per kb, converted to PHYLIP with vcf2phylip to randomly resolve heterozygotes	IQ-TREE phylogeny	207,854 SNPs; 198,618 variable after heterozygote resolution
Snapper dataset	12 North, 3 South (1 bee per population with highest seq coverage), outgroups	IQ-TREE input with individuals removed, 0% missing data, 1 SNP per kb, 5K remaining SNPs randomly selected	Snapper species tree	7,350 SNPs; 5,000 randomly chosen for SNAPPER xml
GADMA dataset	28 North, 9 South	Q = 30, GQ = 20, biallelic, 4% missing (allows 2 missing genotypes per SNP), 1 SNP per kb	GADMA demographic model	301,083 SNPs

sample on results, and the focus of analyses on either individual variation or deeper phylogenetic divergence between regions rather than fine scale population genomics, we elected to retain both samples for analysis (see Results).

Population Structure

We performed a principal component analysis (PCA) using the R package adegenet v2.1.10 (Jombart and Ahmed 2011). We first used the R package vcfR v1.14.0 (Knaus and Grünwald 2017) to read the VCF into R, the command vcfR2genlight to convert the VCF into a genlight object, and the function glPca in adegenet to perform a PCA on the genlight object. To examine population structure, we performed sNMF analysis in the R package LEA v3.8.0, which utilizes sparse non-negative matrix factorization to estimate genetic ancestry (Gain and François 2021). We first used plink v1.90b6.21 (Purcell et al. 2007) to convert the filtered VCF into ped format. We then used LEA to convert the PED file into Geno format. We used the sNMF command in LEA to estimate the number of ancestral populations (K), testing K-values 1 to 10 with 25 repetitions. We then examined the cross-entropy values for each K to determine the best statistically supported number of ancestral populations, examining both the relative change between successive values of K and the minimum cross-entropy value. Based on results showing that $K = 2$ or 3 both had similarly low entropy, we report results for both K values in both SNP datasets (Supplementary Fig. S1). Finally, we calculated Weir and Cockerham's pairwise F_{ST} (Weir and Cockerham 1984) between each locality and population detected by sNMF with the function gl.fst.pop as implemented in the R package dartR v2.9.7 (Gruber et al. 2018).

Genetic Diversity

We used the "high depth" and "full data" SNP datasets to estimate patterns of genetic diversity by first calculating observed (H_O), and unbiased expected heterozygosity (H_E) in each sampling locality using the R package dartR version 2.9.7 (Gruber et al. 2018). The high depth dataset was employed here to evaluate the impact of low coverage SNPs from some museum samples on results (Kardos and Waples 2025). We used the command gl.report.heterozygosity on the genlight object containing the SNP information as described above for the PCA.

As a second metric of diversity, we used the roh command in the package bcftools v1.21. We used the "full data" dataset containing only variant sites and the option -G 30 to obtain runs of homozygosity (ROH) estimates per individual. A ROH is a continuous, unbroken stretch of DNA where an individual has inherited 2 identical copies of the same genetic sequence—one from each parent. To visualize the length distribution of the ROH between individuals in the north and the south we produced geometric density plots in ggplot2 v3.4.4 (Wickham 2011). Following the methodology of previous studies (Robinson et al. 2022, Schweizer et al. 2025), we estimated F_{ROH}, which describes the proportion of the genome that is contained within a ROH of a given size. First, we constructed a pseudogenome containing only homozygous sites on the "full data" vcf. Next, we estimated F_{ROH} using 3 different ROH length cutoffs: 10 kb, 100 kb, and 1 Mb.

Unbiased Whole-Genome Population Structure and Diversity

To better take advantage of the whole genome dataset for estimating genetic diversity at a genome-wide scale, we calculated nucleotide diversity (π), genetic divergence (d_{xy}), and F_{ST} using

the unbiased estimator pixy v1.2.10 (Korunes and Samuk 2021). In the presence of missing data typical of whole genome data sets, estimates of genetic diversity and divergence can be biased (Korunes and Samuk 2021). Pixy produces unbiased estimates of genetic diversity from whole-genome data (Korunes and Samuk 2021) by accounting for missing data in calculations, producing more accurate estimates of population genetic statistics. Using the "all sites" VCF containing both variant and invariant sites, we used pixy to calculate genome-wide estimates of nucleotide diversity (π), genetic divergence (d_{xy}) and F_{ST} in non-overlapping 10,000 bp windows, grouping samples into North (United States and Canada) and South (Mexico) genetic populations identified as the major $K = 2$ split from the sNMF analysis. We removed any windows containing <5,000 sequenced sites for π and d_{xy} and windows with fewer than 10 SNPs for F_{ST}.

Phylogenetic Analyses

SNP-Based Phylogenies

We used the genotyping from GATK as above for the phylogenetic SNP set, however we retained sequences from outgroups in addition to the *B. huntii* samples. Note that *B. vancouverensis* and *B. bifarius* are recently redescribed sister species and provide some calibration of expected levels of divergence for recently isolated species (Ghisbain et al. 2020). We applied several filters to prepare data for different analyses. First, we generated a maximum likelihood phylogeny with 1,000 ultra-fast bootstraps using IQ-TREE v2.2.5 (Minh et al. 2013, Hoang et al. 2018). The SNP set used with IQ-TREE was filtered from the raw GATK output VCF using VCFTools as above to include 207,854 biallelic SNPs with a minimum base quality of 30, a minimum genotype quality of 20, a minor allele count of 2, a maximum of 20% missing data, and thinned to 1 SNP per kb. The filtered VCF was then converted to PHYLIP format for the IQ-TREE input using the Python program vcf-2phylip.py (Ortiz 2019) using default settings except for specifying one of the *B. impatiens* samples as the outgroup (IN08_0492_impatiens) and randomly resolving heterozygous sites to avoid IUPAC ambiguities. This produced an alignment with 197,618 remaining variable sites after resolving heterozygotes (158,947 parsimony-informative and 39,671 singleton SNPs). We determined the best model using ModelFinder (Kalyaanamoorthy et al. 2017) as part of the IQ-TREE analysis (the best-fitting model was TVM + F+ASC + R5 using BIC, AIC, and AIC_C). We visualized the consensus tree and ultra-fast bootstrap support with FigTree v1.4.4 (Rambaut 2018).

Second, we used SNP data for a multi-species coalescent (Maddison 1997) based species-tree and divergence time analysis using the BEAST2 v2.7.5 (Bouckaert et al. 2019) package SNAPPER v1.1.3 (Stoltz et al. 2021), a diffusion-model version of the Bayesian species tree inference approach in SNAPP v1.6.1 (Bryant et al. 2012). We generated an input file for SNAPPER by filtering the raw GATK output as for IQ-TREE. To reduce computation time in SNAPPER, we reduced the data complexity by subsampling both the sample size and number of SNPs from the IQ-TREE input file with the goal of generating an input with ~5,000 to 10,000 SNPs with no missing data: we retained the one *B. huntii* sample per locality with the most complete data, removed all SNPs with any missing data, and filtered loci to one SNP per 25 kb, which produced 7,351 biallelic SNPs with no missing data. For analyses, we largely followed approaches described the "Divergence-Time Estimation with SNP Data" tutorial by M. Matshiner (https://github.com/ForBioPhylogenomics/tutorials/tree/main/divergence_time_estimation_with_snp_data) (also see Stange et al. 2018). We prepared SNAPPER input XML files using the included snapp_prep.rb ruby script (https://github.com/mmatschiner/snapp_prep), which employs settings optimized for species divergence time analyses (see Stange et al. 2018 for parameter and operator selection details). We specified an assignment input file to group samples to species, subdividing *B. huntii* into northern (United States + Canada, $n = 12$) and southern (Mexico, $n = 3$) groups based on the PCA and $K = 2$ sNMF results (see Results), and retaining all outgroups ($n = 2$ for each). We specified 1 age constraint based on prior estimate of divergence time between *B. impatiens* from the remaining taxa using a normal distribution with an offset of 0, a mean of 13.0086 Ma from the recent time-calibrated biogeographic analysis of most *Bombus* species in Santos Júnior et al. (2022), and a standard deviation of 1.5 Ma in the constraint file to approximate the credible interval from Santos Júnior et al. (2022). Because there are some conflicting divergence estimates in the literature for this group of *Pyrobombus* (Hines 2008, Santos Júnior et al. 2022), we also repeated the analyses using the more recent 6.35 Ma calibration date constraint for the *B. impatiens* divergence from Hines (2008). We ran the snapp_prep.rb script with the -a SNAPPER option and randomly retained 5,000 SNPs (integer format, homozygotes 0 or 2 at random) with a chain length of 750,000 MCMC iterations (store every 100) and the XML file was run using BEAST2 using 2 independent replicates. The resulting logs were visualized with TRACER v1.7.2 (Rambaut et al. 2018) to evaluate the MCMC chain stationarity after removing 10% of iterations as burn-in; all ESS values were >200 in each run, indicating that a sufficient number of MCMC iterations was performed. For each run, 10% of iterations were discarded as burn-in and the chains were combined. The resulting trees were summarized with TreeAnnotater v2.7.5 and posterior support values and node ages with 95% HPD intervals were visualized with FigTree v1.4.4.

UCE Phylogeny

Third, because above analyses utilized SNP-only data, we also wanted to evaluate a locus-based approach using full sequences for a set of well-characterized phylogenetic markers that have been widely used in the systematics of Hymenoptera (Branstetter et al. 2017a, 2017b, Almeida et al. 2023, Blaimer et al. 2023, Wutke et al. 2024, Rohde et al. 2025). We thus employed analysis of ultraconserved elements (UCEs), an established approach for inference of species-level phylogenetics in bees with a well-documented set of loci (e.g. Rohde et al. 2025). We first *de novo* assembled the raw sequence data for *B. huntii* using SPAdes v3.14.1 (Bankevich et al. 2012) and extracted (UCE) loci using Phyluce v1.7 software (Faircloth 2016) following an established workflow (https://phyluce.readthedocs.io/en/latest/tutorials/tutorial-3.html). For this process, we aligned the available Hymenoptera bait set (Branstetter et al. 2017b; Hym-v2 principal) to the assemblies using min-coverage and min-identity, both set at 80, and sliced out 500 bp of flanking sequence. We repeated the process for outgroup genomes from NCBI: *Bombus impatiens* (GCA000188095), *B. bifarius* (GCA011952205), *B. vancouverensis* (GCA011952275), and

2 genomes of *B. vosnesenskii* (GCA011952255, GCA026744215). We assessed the number of recovered loci and the length of each locus for each taxon using a Phyluce script (*phyluce_assembly_get_fasta_lengths*).

Following the extraction of UCE contigs, we removed paralogs using Phyluce (*phyluce_assembly*_match_contigs_to_probes), aligned the data using MAFFT, and trimmed the alignments using Gblocks (Talavera and Castresana 2007), with reduced stringency settings (b1 = 0.5, b2 = 0.5, b3 = 12, b4 = 7). We filtered the alignments to have 75% taxon completeness and inferred an initial phylogenetic tree using IQ-TREE v2.2 (Minh et al. 2020). Following this initial analysis, we decided to further trim the dataset using Spruceup v2024.7.22 (Borowiec 2019), which trims outlier sequences from individual samples. For this analysis, we used a rooted cladogram as a guide tree and the Weibull distribution. We tested several cutoff values, but ultimately selected 0.9999999999999 as the best value for this dataset. Following trimming, we split loci using AMAS (Borowiec 2016) and removed empty columns using a custom script (https://github.com/marekborowiec/remove_empty_columns). We then filtered the data for 50% taxon completeness and generated summary statistics using Phyluce (phyluce_align_get_align_summary_data).

To infer the final UCE tree, we partitioned each locus into regions using the sliding window site characteristics based on entropy (SWSC-EN) method (Tagliacollo and Lanfear 2018) as implemented in the program CURE (Freitas et al. 2021). We then merged loci with ModelFinder2 within IQ-TREE using the rclusterf 10 algorithm and the GTR + G model of sequence evolution. Following model merging, we conducted an unrooted, partitioned analysis of the data with full model selection (-m MFP) and assessed support using ultrafast bootstrap (UFB) replicates (Hoang et al. 2018) and SH-like branch tests (Guindon et al. 2010), with 1,000 replicates for each. We rooted the final tree on *B. impatiens*.

Testing for Migration With Divergence

Based on results suggesting a primary split into 2 major population clusters or phylogenetic clades representing the Northern (United States + Canada) and the Southern (Mexico) localities (see Results), we were interested in testing for ongoing gene flow between these *B. huntii* groups. Our primary goal was to test the hypothesis that migration rates were significantly greater than zero and to evaluate divergence time using a direct mutation rate estimate in comparison to phylogenetically inferred constraints used in SNAPPER. We performed demographic analyses using a 2-population isolation with migration model in GADMA 2.0.0 (Noskova et al. 2022). GADMA is a flexible approach for demographic inference from site frequency spectrum (SFS) data. GADMA uses a genetic algorithm to perform unsupervised parameter estimation and model selection under a given demographic model structure and can utilize different likely engines that are widely used for inference with SNP data, such as ∂a∂i (Gutenkunst et al. 2009) or MOMENTS (Jouganous et al. 2017). To prepare data for GADMA, we first generated a site-frequency spectrum (SFS) file from SNP data above. We used the initial filter VCF file from above, which had been filtered for poor quality SNPs but not based on minor allele frequency. To balance the number of SNPs, completeness of the data matrix, and number of retained samples in SFS down-projection, we thinned the data to retain one SNP with ≤6% missing data (equivalent to allowing 2 missing samples and ensuring representation of each locality) per kb ($N = 86{,}782$ SNPs). To account for remaining missing data we down-projected the SFS by selecting the sample size in each population (52 gene copies in the northern population and 14 in the Mexican population) that maximized the number of segregating sites (Gutenkunst et al. 2009) as determined using easySFS v 0.0.1 (https://github.com/isaacovercast/easySFS). We employed the MOMENTS (Jouganous et al. 2017) engine within GADMA and specified an isolation-with-migration demographic model where an ancestral population split into the 2 contemporary populations (parameter setting Initial Structure: 1,1), that were each allowed to undergo a sudden, linear, or exponential size change and experience asymmetrical migration. The best model was selected using AIC (parameter setting Linked SNPs: FALSE). We performed 60 simultaneous replicates to identify the best model. Parameters were scaled from genetic units to real world values (e.g. time in years, populations sizes in numbers of individuals) using a direct mutation rate (μ) estimate for bumble bees of 3.6×10^{-9} per site per year (Liu et al. 2017) and an effective sequence length (L) that corrects the total size of the genome by the proportion of total SNPs removed by filtering for missing data or thinning, calculated as specified in the GADMA manual, as follows. The total length of the *B. huntii* genome scaffolds analyzed was 279,265,701 bp, and the number of initial SNPs (filtered only for quality as above, but not for missing data) was 9,520,747. The final number of SNPs in the thinned data set was 86,782, of which 39,796 were retained in the downsampled SFS. Thus, L was estimated as [(39,796/9,520,747) * 279,265,708] = 1,167,309 effective bp. We generated bootstrapped 95% confidence intervals (CIs) for the AIC-selected MOMENTS model parameter estimates using the functions gadma-run_ls_on_boot_data and gadma-get_confidence_intervals from 200 pseudoreplicate SFS generated as above from VCF files containing randomly resampled SNPs, following the GADMA manual (gadma.readthedocs.io/en/latest/user_manual/confidence_intervals.html). Finally, parameter estimates and CIs in real-world units were adjusted to account for haplodiploidy (only 0.75 chromosome copies per individual) in bumble bees by calculating the reference effective population size as $Theta/(3*\mu*L)$ and using the equations provided in the GADMA manual (gadma.readthedocs.io/en/latest/user_manual/units.html; see also Gutenkunst et al. 2009). After the simple isolation with migration model indicated post-divergence gene flow, we were interested in testing if migration had only occurred during early post-divergence or might be ongoing. We repeated the GADMA analysis by adding a second post-divergence phase by specifying "Initial structure: 1,1" and "Final structure: 1,2" in the parameter specification file (adding a second post-divergence time greatly increased early migration rates, so upper bounds had to be increased to Max_M: 50). Because of small sample sizes, we were concerned that estimation of the greater number of parameters in this 2-phase post-divergence model might be challenging for SFS data (e.g. see https://gadma.readthedocs.io/en/latest/faq.html), and thus we consider this

2-phase model as secondary to the simpler isolation-with-migration model above.

Results

DNA Barcoding

The 29 newly sequenced and 17 GenBank samples produced seven 516 bp haplotypes with 6 segregating sites. All haplotypes were related by a series of single nucleotide differences (Fig. 2A). Most samples ($n = 32$) that were all from the United States and Canada, shared a single haplotype that was a central node in the TCS network (Haplotype D). Three additional COI sequences (Haplotypes A to C) were found in 9 other US and Canadian samples, all one bp different from this central Haplotype D sequence. The 5 sequenced Mexico samples had 3 unique haplotypes (E to G) that formed a group that collectively was one bp different from the US + Canada haplotype group (A to D), with a mean raw percent sequence difference between the Mexico and US + Canada samples of 0.35%.

Population Structure and Diversity

The PCA split the United States and Canada individuals from Mexican samples along PC1 (13.0%) and split individuals from the Chihuahua locality in northern Mexico from the rest along PC2 (10.3%) (Fig. 2B). Cross-entropy (CE) analysis in sNMF on the "low missing data" dataset was similar, indicating that $K = 2$ had the lowest CE value, indicating 2 as the most likely number of major genetic populations, although both $K = 2$ and 3 were similar, so both values are shown (Fig. 2C and D). The sNMF $K = 2$ analyses clustered samples into a northern (US and Canada) and southern (Mexico) genetic population. The $K = 3$ analysis showed a further subdivision of the Mexico genetic population by separating the Chihuahua samples from Nuevo Leon and Puebla samples (Fig. 2D). sNMF and PCA analyses on the "full" dataset exhibited identical patterns to the "low missing data" dataset presented here (Supplementary Figs S2 and S3).

Pairwise F_{ST} by sampling locality indicates low population divergence within the United States and Canada, with values ranging from 0 to 0.1 (Table 2), consistent with the sNMF and PCA analyses. Comparisons between the north (US and Canada) and south (Mexico) sampling localities showed elevated divergence (ranging from $F_{ST} = 0.26$ to 0.47). Finally, the pairwise comparisons within the Mexico sampling localities showed the localities within Mexico were as differentiated or exhibited greater differentiation between the 3 localities as between the localities in the United States and Canada, with F_{ST} values ranging from 0.46 to 0.66. Regional values estimated for the sNMF clusters also were consistent with large differentiation among southern and northern populations and within-Mexico (Fig. 2C and D), but values were lower, suggesting some upward bias in F_{ST} from small-sample sizes for the locality-specific comparisons.

Using the "full dataset," the northern sampling localities exhibited higher levels of unbiased H_E (ranging from 0.18 to

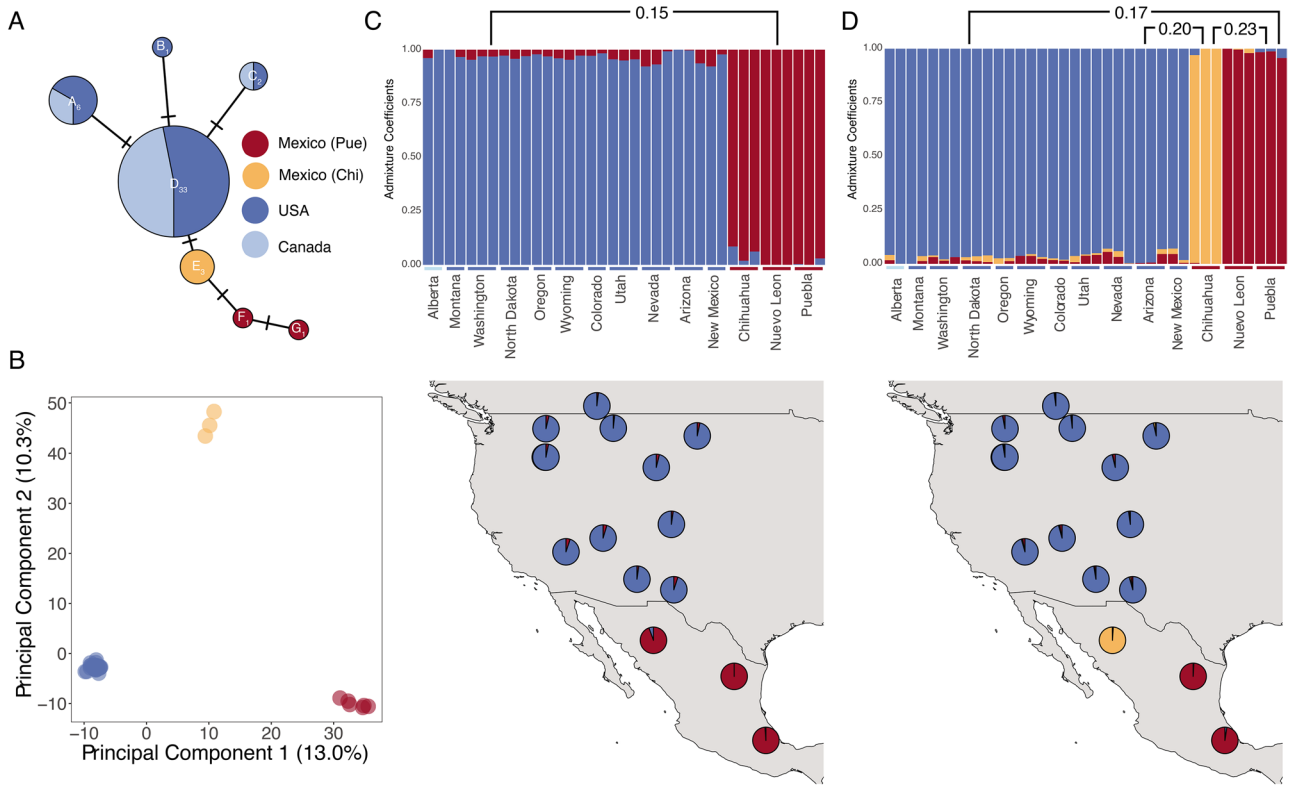

Fig. 2. Mitochondrial COI network and analysis of population structure with PCA and sNMF. (A) Haplotype TCS network with each letter indicating a unique haplotype (subscripts indicate number of sequences belonging to that haplotype) colored by geographic region, with 2 regions of Mexico based on results from (D). (B) PCA for the "Low Missing Data" dataset showing the first 2 principal components that explain the greatest amount of variation. Points are colored corresponding to the sNMF $K = 3$ results. (C) Shows sNMF $K = 2$ analysis and (D) $K = 3$ analysis with the bar graphs indicating admixture coefficients per individual ordered by latitude and maps showing the average admixture coefficient at each sampling locality ("Low Missing Data" dataset). The brackets above the bar graphs indicate pairwise F_{ST} values between the respective regions in both (C) and (D).

Table 2. Pairwise F_{ST} by sampling locality using the "Full" SNP dataset from Table 1

	North Dakota (N)	Alberta (N)	Nevada (N)	Washington (N)	Oregon (N)	Utah (N)	Arizona (N)	Wyoming (N)	Colorado (N)	New Mexico (N)	Montana (N)	Puebla (S)	Nuevo Leon (S)
Alberta (N)	−0.0008												
Nevada (N)	0.0330	0.0374											
Washington (N)	0.0032	−0.0019	0.0064										
Oregon (N)	0.0041	−0.0037	0.0333	−0.0054									
Utah (N)	−0.0009	−0.0037	0.0311	0.0015	0.0004								
Arizona (N)	0.0712	0.0950	0.1302	0.0778	0.0763	0.0692							
Wyoming (N)	−0.0003	−0.0004	0.0336	0.0039	0.0039	−0.0017	0.0685						
Colorado (N)	−0.0012	−0.0042	0.0353	−0.0012	−0.0020	−0.0023	0.0910	−0.0003					
New Mexico (N)	0.0049	−0.0009	0.0352	0.0051	0.0002	0.0023	0.0947	0.0056	−0.0006				
Montana (N)	0.0003	−0.0033	0.0311	0.0010	−0.0001	−0.0009	0.0813	0.0015	−0.0032	−0.0098			
Puebla (S)	0.3379	0.4211	0.4689	0.3437	0.3980	0.3375	0.4166	0.3342	0.4034	0.4083	0.3637		
Nuevo Leon (S)	0.2983	0.3712	0.4156	0.3051	0.3528	0.2980	0.3750	0.2937	0.3557	0.3622	0.3225	0.6620	
Chihuahua (S)	0.2666	0.3389	0.3881	0.2728	0.3180	0.2652	0.3495	0.2625	0.3216	0.3272	0.2898	0.6554	0.4561

0.23) than the southern sampling localities (H_E = 0.06 to 0.08) (Fig. 3A). H_O calculated per individual ranged from 0.27 to 0.37 in the north and from 0.08 to 0.14 in the south (Supplementary Data File S1; Fig. 3B). To ensure that these estimates were not an artifact of sequencing depth (Kardos and Waples 2025), we repeated calculations with the high depth dataset imposing a minimum sequencing depth of 15× and observed similar trends, with the southern samples exhibiting decreased levels of unbiased H_E per sampling locality and H_O per individual compared to the northern samples (Supplementary Data File S1; Supplementary Fig. S4). To quantify levels of inbreeding, we performed an analysis of ROH per individual. Northern samples exhibited a mean of 160 ROH with a mean ROH length of 52,250 bp. Southern samples exhibited significantly more and longer ROHs ($P < 0.001$), with a mean of 1,617 ROH and a mean ROH length of 70,194 (Fig. 3C). To understand the proportion of the genome that was made up of ROH, we estimated the F_{ROH} with 3 different ROH length cutoffs: >1 Mb, >100 kb, and >10 kb. The individuals in the south consistently showed increased F_{ROH} values, indicating increased levels of inbreeding across the 3 sampling localities (Fig. 3D).

In the pixy analysis, the genome-wide estimate of F_{ST} suggested a moderate amount of divergence with a global value of 0.15 (Fig. 4; note this level is reduced from SNP-based F_{ST} values above owing to a lack of a MAF filter). There was a consistent pattern of divergent peaks at the tails of the chromosomes but was otherwise fairly constant across the genome. The genome-wide estimate of genetic divergence among all samples using absolute divergence d_{xy} was 0.0021 and was likewise consistent across chromosomes but without many of the spikes in F_{ST}, especially near chromosome ends, suggesting these spikes were likely associated with regions of reduced diversity. The within-population estimation of genetic diversity using π suggested slightly higher genetic diversity in the north, with the combined northern population exhibiting a π of 0.0019 and the combined southern population exhibiting a pi of 0.0016, with the northern population consistently more diverse across the length of each chromosome.

Phylogenetic Analyses, Divergence Times, and Demographic Modeling

The IQ-TREE maximum likelihood phylogeny of the SNP dataset recovered the known existing relationships of included species, with each species monophyletic with 100% ultrafast bootstrap (UFB) support (Fig. 5A). Within *B. huntii*, 2 monophyletic clades were recovered: a southern Mexican clade with 100% UFB support and a northern clade including the US + Canada samples that only had 86% UFB support. The branch separating these 2 clades was also notably shorter than between the other recently separated species pair of *B. vancouverensis* and *B. bifarius* (Ghisbain et al. 2020). Interestingly, the 3 Mexican localities were each recovered as monophyletic (all 100% support) within the southern clade, with Chihuahua sister to Nuevo Leon and Puebla; no similarly strong geographic structuring was apparent within the northern clade apart from the 3 Arizona samples.

The UCE-based ML tree (Fig. 5B) also grouped the Mexican samples into a monophyletic clade with maximum support (100/100 UFB/SH-aLRT); however, this clade was nested within a paraphyletic assemblage comprising the remaining US and Canada samples. Within the Mexican clade, the 3 localities

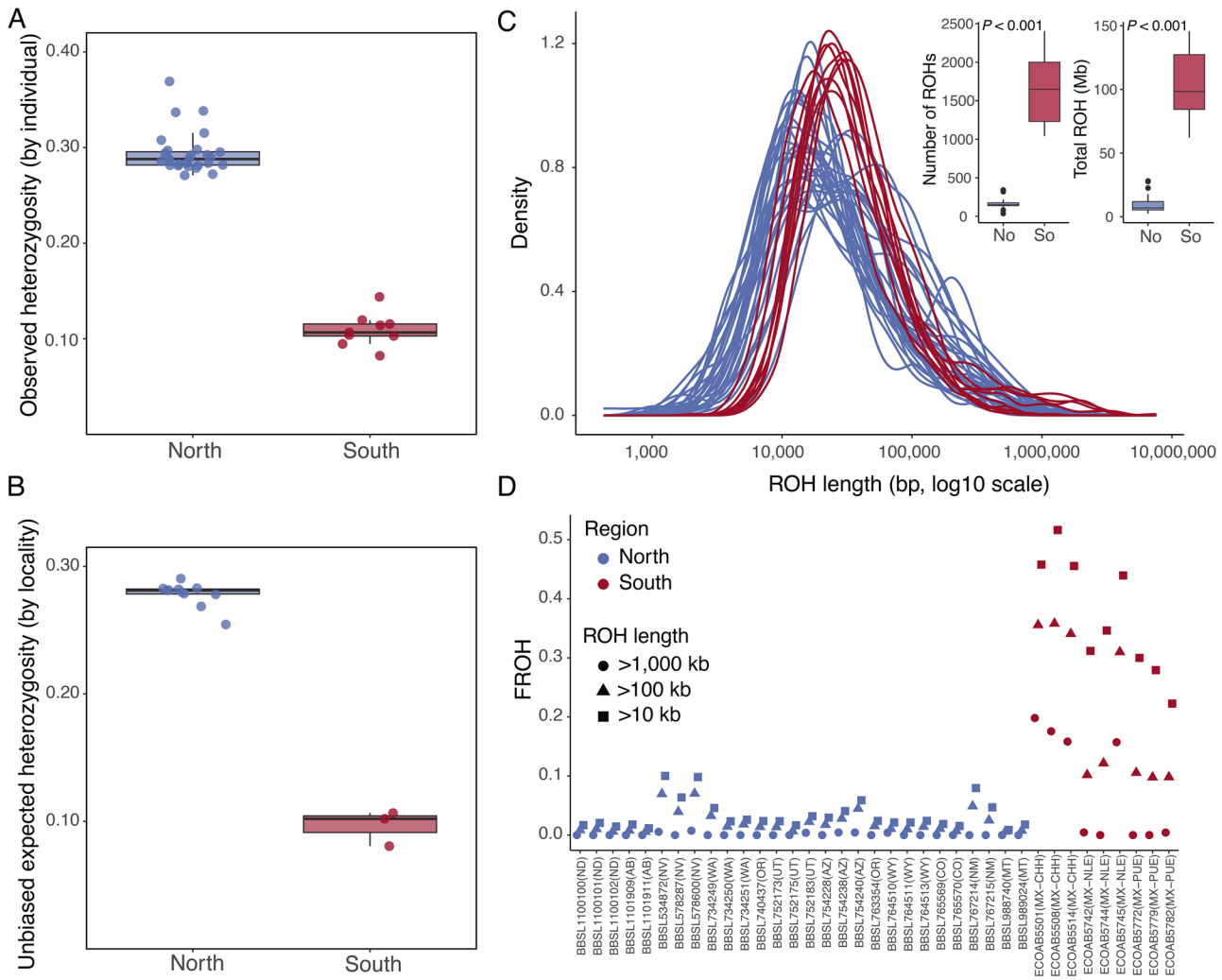

Fig. 3. Observed and unbiased heterozygosity and runs of homozygosity (ROH) for the "Full" dataset. (A) Observed heterozygosity per individual separated by geographic region. The top and bottom of the boxplots represent the third quartile and first quartile of values, respectively, with the line inside the box representing the median value. The upper and lower whiskers extend to the furthest datapoints that are not greater than 1.5 times the interquartile range, with points extending beyond the whiskers considered as outliers. Points reflect values for each individual sample. (B) Unbiased expected heterozygosity per sampling locality separated by geographic region; boxplots as in (A) except points reflect values for each locality. (C) A density plot of log-transformed ROH distribution colored by geographic region. The inset shows the differences in number of ROH and total ROH between the northern and southern populations tested with Wilcoxon rank-sum tests in R; boxplots as in (A), except points indicate outlier values. (D) F_{ROH} values by geographic region with 3 different ROH length cutoffs identified by shape: >1 Mb, >100 kb, and >10 kb.

were each recovered as monophyletic (all 100/100 support), with Chihuahua sister to Nuevo Leon and Puebla as in the SNP-based results. The paraphyletic northern group of samples showed little geographic structuring and most internal nodes received support values below 100/100.

For the SNAPPER coalescent population tree analysis, all nodes had 100% posterior support (Fig. 5C). The divergence times scaled by the *B. impatiens* constraint of 13 Ma (inferred by SNAPPER to a mean of 12.73 Ma) were similar to the species-level divergence times from the *Bombus* phylogeny reported by Santos Júnior et al. (2022). The split for northern and southern *B. huntii* populations (corresponding to populations in the $K=2$ sNMF analysis above) was inferred as 0.47 Ma (0.35% to 0.59 95% HPD), which is more recent than the inferred *B. vancouverensis-B. bifarius* split of 1.18 Ma (0.88% to 1.50 95% HPD). The dates on the SNAPPER tree are dependent on the constraint date provided, with the Hines (2008) divergence calibration of 6.35 Ma for the *B. impatiens* split placing SNAPPER node ages of other species divergences in line with Hines (2008), and the age of the *B. huntii* north-south divergence at 0.22 Ma (0.17% to 0.27 95% HPD) (Fig. 5C). The top GADMA model for both log-likelihood and AIC included gene flow between the northern and southern lineage, with the final model indicating a large ancestral population dividing into smaller contemporary lineages and with significantly positive ongoing gene flow biased in the south-to-north direction, although the 95% CI for the north-to-south rate included zero (Fig. 5D). The estimated divergence time of 0.183 (95% CI: 0.172 to 0.198) Ma from the direct *Bombus* mutation rate was more recent than the lower bound from SNAPPER using the Santos Júnior et al. (2022) constraint age but overlapped the 95% HPD for the 0.22 Ma divergence from the Hines (2008) constraint. The secondary 2-phase post-divergence model selected by AIC indicated that migration was likely to be much greater in the ancestral post-divergence period (again driven by extensive south-to-north gene flow), with a second

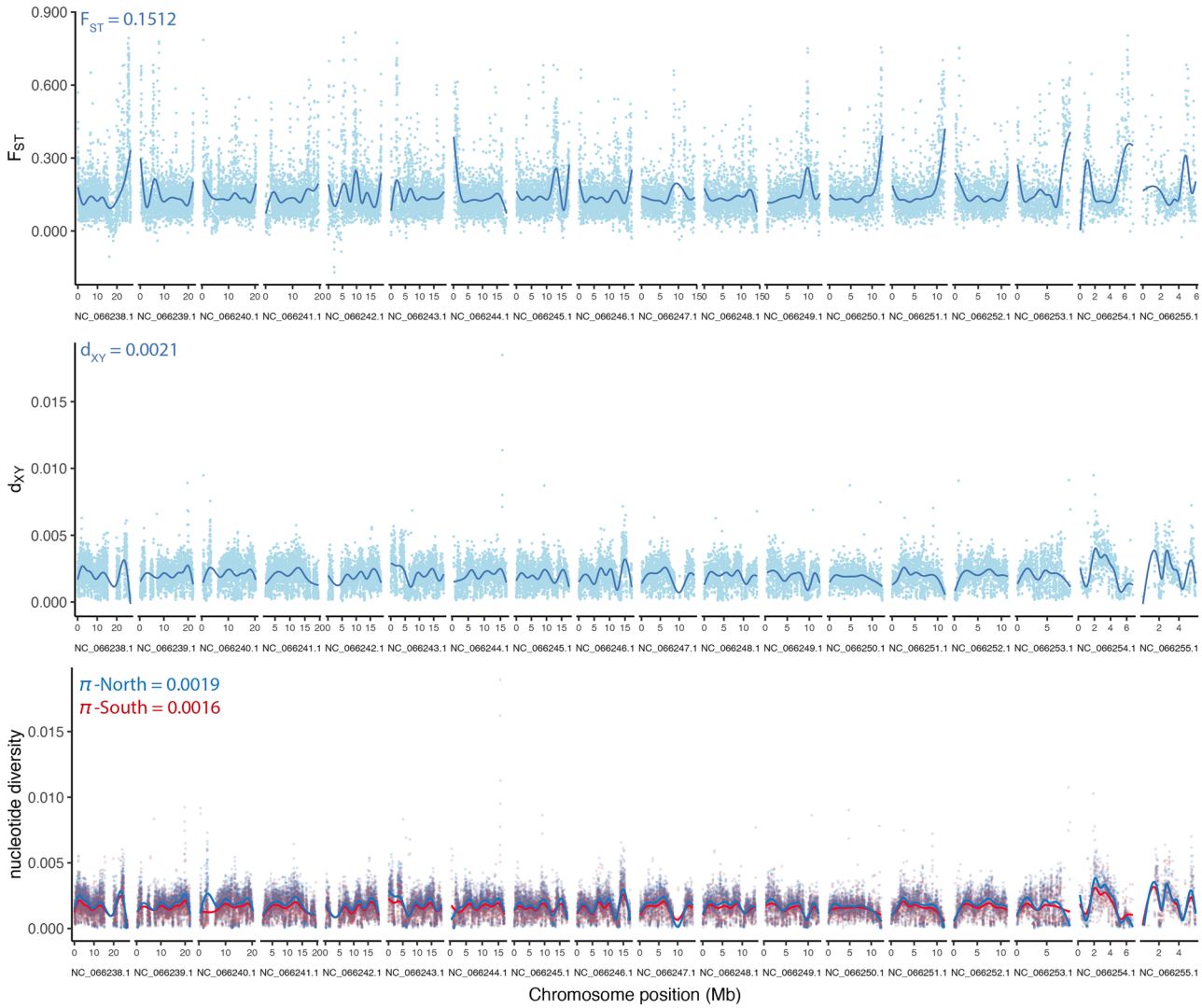

Fig. 4. Genome-wide estimates of nucleotide diversity (pi), d_{xy}, and F_{ST} across the 18 chromosomes ("All Sites" dataset). The figures given in the top left of each analysis indicate the value averaged across the genome. The colors for the nucleotide diversity values correspond with geographic region.

phase identified to start approximately 54,000 yr before present that was characterized by a cessation of ongoing gene flow (Supplementary Fig. S5).

Discussion

We used a museomics approach to resequence whole genomes from the widespread bumble bee *B. huntii*, taking advantage of the new reference genome assembly for this species (Koch et al. 2024). We reexamined previously identified population structure and genetic diversity gradients across the species' geographic range (Koch et al. 2018) and evaluated the hypothesis that *B. huntii* found in Mexico might warrant classification as a separate species from the US and Canada populations that was based on strong differentiation observed in prior work (Koch et al. 2018). We found evidence of strong population structure between the northern and southern populations alongside little differentiation among northern localities but substantial differentiation among localities within Mexico. Southern *B. huntii* also exhibited relatively low levels of genetic diversity. Despite this population structure, phylogenomic analyses did not strongly support splitting the populations into different species; although bees from the United States + Canada and Mexico formed monophyletic clades in the SNP-based phylogeny, the northern branch was not highly supported (86% UFB support) and the 2 regions were not reciprocally monophyletic in the UCE phylogeny, although we acknowledge that biological species can be paraphyletic due to incomplete lineage sorting (Funk and Omland 2003). Further, demographic analysis with an isolation-with-migration model in GADMA indicated post-divergence gene flow between the northern and southern populations, although the current distribution of suitable habitat has likely greatly reduced or eliminated more recent migration. Thus, we hypothesize that the genetic differences observed are likely explained by greater geographic isolation and high rates of genetic drift in southern *B. huntii* that are driven by partial isolation at higher elevations in this region (Fig. 1). We argue that there is not currently strong evidence

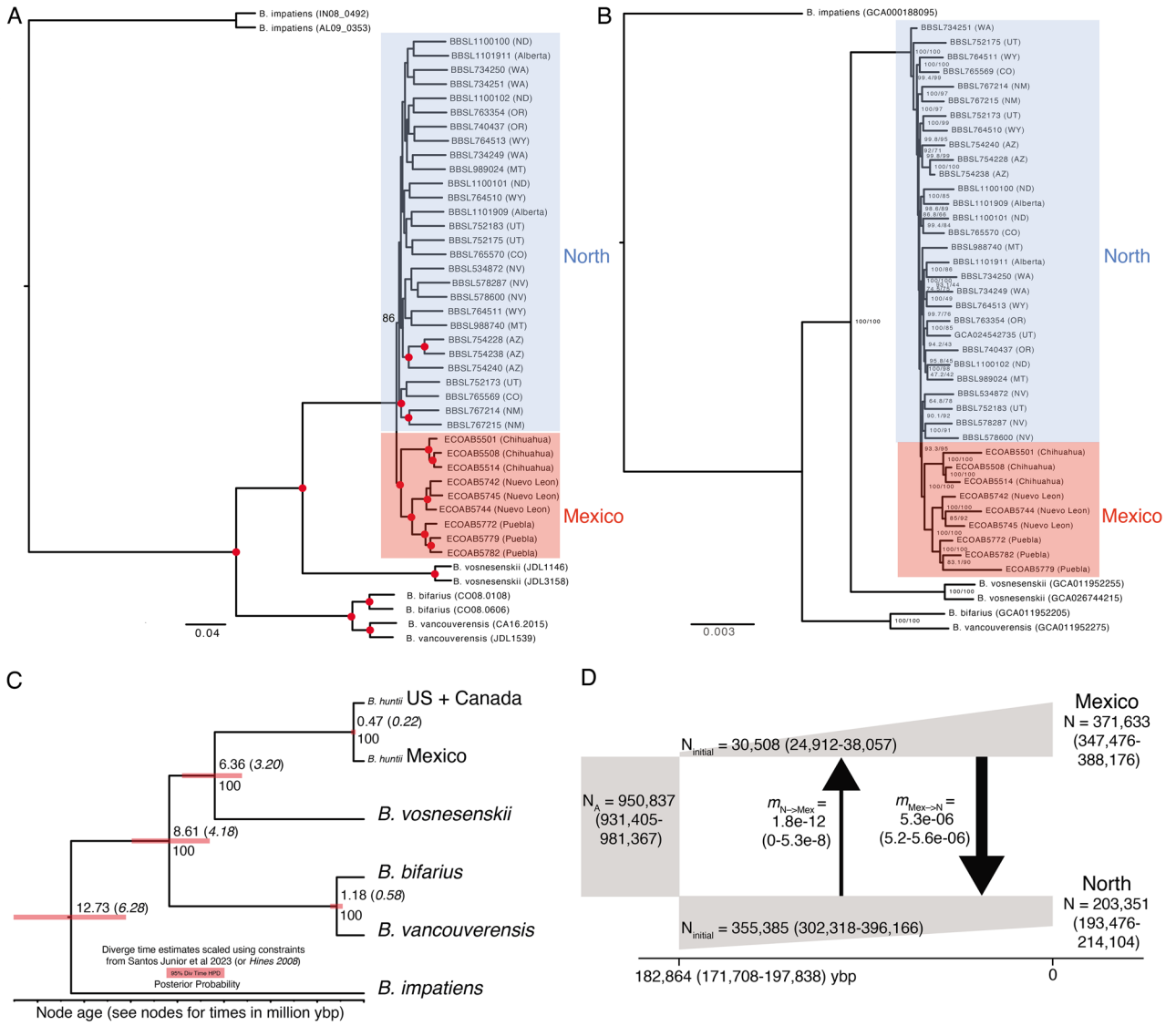

Fig. 5. Phylogenetic and phylogeographic analyses of *B. huntii* populations. (A) IQ-TREE maximum-likelihood SNP-based phylogeny, with the 2 main *B. huntii* lineages (North and Mexico) indicated with population genetic analyses shaded as in Fig. 2C. Red node symbols indicate 100% ultrafast bootstrap (UFB) support, with 86 indicating support for the monophyletic North clade. (B) UCE-based IQ-TREE maximum likelihood tree, shown as in (A), with node support given as UFB/SH-aLRT. (C) SNAPPER species tree for outgroups and the 2 main *B. huntii* lineages. Node values indicate divergence time in million years before present (upper; values from Santos Júnior et al. [2023] constraint age first, and from Hines [2008] constraint age in parentheses and italics), posterior support (lower), and error bars indicating 95% posterior density divergence time intervals. (D) The best-fitting demographic model estimated using the MOMENTS engine in GADMA2, including estimates of divergence time (*T*), population sizes for the ancestral population (*NA*), initial post-divergence population sizes ($N_{initial}$), current population sizes (*N*) and asymmetric migration rates (*m*), with the values and arrows indicating the proportion of individuals migrating into the respective population per generation.

in favor of splitting the northern and southern *B. huntii* populations into separate species (Chambers et al. 2025). However, our results improve our understanding of how Quaternary climatic processes have shaped population structure and genetic diversity in bumble bees.

Population Structure and Diversity Patterns

Population structure estimates between the northern and southern populations are consistent with the results from a prior range-wide microsatellite study of *B. huntii* (Koch et al. 2018). Clustering analyses supported a broad northern genetic cluster consisting of all individuals from the United States and Canada and a southern genetic cluster containing the individuals from Mexico. The northern population consistently exhibited greater levels of genetic diversity within every level of organization that we examined (whole-genome, individual, and locality) compared to the southern population, and different filtering and quality assessment approaches suggest that such differences are not driven by differences in sequencing coverage or other artifacts (Supplementary Fig. S4). The northern population also exhibited lower levels of inbreeding according to ROH estimates, showing fewer and shorter ROH compared to the southern population. Additionally, the southern population demonstrated greater F_{ROH} among all ROH size cutoffs, indicating that a greater proportion of the genome is made up of ROH than in the northern population, which is consistent with populations that are geographically isolated (Gmel et al. 2023,

Zarn et al. 2025). These patterns of decreased levels of genetic diversity and increased population structure in the southern part of the species range have been demonstrated before in other bumble bee species including *B. vancouverensis* and *B. flavifrons* (Lozier et al. 2023, Sakulich et al. 2025) and are consistent with the prior findings in *B. huntii* in Koch et al. (2018). There has been an increased focus on documenting range wide patterns of genetic diversity and population structure in bumble bees (Koch et al. 2018, Mola et al. 2024, Gornall et al. 2025, Sakulich et al. 2025), and the results presented here largely correspond with what has been found in recent studies of bumble bee species with similar geographic ranges compared to the minimal population structure that has been identified in bumble bee species with more continuous geographic distributions (Christmas et al. 2022, Heraghty et al. 2023).

The southern ranges of *B. huntii* and several other North American taxa mentioned above, such as *B. vancouverensis*, tend to be restricted to higher elevation habitats, which results in greater geographic isolation and reduced gene flow through low-lying areas. In the northern parts of these ranges, species exhibit higher levels of range connectedness, reducing population structure. In the case of *B. huntii*, historical climatic patterns played a significant role in geographically isolating the southern populations, as populations would have moved upslope to track suitable climatic conditions in southern montane regions during warming periods (Koch et al. 2018). Thus, the present-day distribution of *B. huntii* in Mexico is much more fragmented than in the United States + Canada but would have been much more connected during glacial periods (Koch et al. 2018). The elevated divergence between the southern and northern *B. huntii* populations, including the recent cessation of gene flow in the secondary GADMA model and further reflected by elevated F_{ST} within the Mexican region, likely indicates geographic isolation and elevated genetic drift associated with restriction to these higher-elevation montane portions of the southern *B. huntii* distribution. This model would also explain the somewhat counterintuitive result that in species like *B. huntii* and *B. vancouverensis*, populations that have experienced greater habitat stability through Pleistocene climate shifts nevertheless maintain lower levels of genetic diversity than populations in northern regions (Koch et al. 2018, Lozier et al. 2023).

Phylogenomics

We hypothesized that the genetic differences observed using microsatellites indicated that *B. huntii* in the southern part of its range could potentially represent a separate species from *B. huntii* in the north, as has previously been observed in other bumble bees such as *B bifiarus*/*B. vancouverensis* (Ghisbain et al. 2020). We did observe genetic differences between the 2 populations; however, the phylogenomic analyses did not provide unambiguous support for speciation, especially when compared to similar bumble bee species that have recently diverged (Ghisbain et al. 2020). The southern population was recovered as monophyletic in the Maximum Likelihood SNP tree, as was each locality within Mexico, but reciprocal monophyly of the northern clade was not strongly supported. The same clade in the UCE tree was found to be paraphyletic. Although UCEs have been applied to resolve species-level questions in bumble bees (Rohde et al. 2025), UCEs are highly conserved regions that may still have power to detect monophyly for very recent divergence, as may be the case for the northern and southern populations. That said, the UCE tree did recover the individual Mexico localities as monophyletic, as in the SNP tree (Fig. 5A and B). An additional possible explanation for the lack of strong support for reciprocal monophyly among the 2 regions, the best-fitting demographic models indicated the presence of non-zero post-divergence gene flow.

The exact timing of the *B. huntii* population divergence in the species tree analysis was dependent on the calibration point used; the calibration based on Santos Júnior et al. (2022; 13.0 ma for the age of the split from the outgroup *B. impatiens*) placed the divergence considerably older than that of Hines (2008; 6.35 ma for the split from *B. impatiens*). However, the isolation-with-migration demographic analysis, which used a direct mutation rate estimation for *Bombus*, matched the divergence estimate using the Hines (2008) calibration, placing the divergence around 180 to 220k ybp. Regardless of calibration dates, the estimated divergence is too ancient to be explained by transitions between the last glacial maximum and the current warmer period (see Koch et al. 2018). Thus, the initial period of divergence would likely have occurred with distributional shifts in association with earlier Quaternary climate cycling. However, we hypothesize that this initial divergence would have included some ongoing gene flow that may have been reduced or eliminated by the more recent niche shifts since the last glacial period. Notably, this timing estimate for the north-south *B. huntii* split is similar to the inferred dates during which northern and southern populations within *B. vancouverensis* began to exhibit diverging demographic trajectories across their western US distribution (Lozier et al. 2023), suggesting that climate shifts during this period may have likewise affected *B. huntii* populations in the region. The GADMA models also indicated some complexity in effective population sizes during and after divergence, with especially strong bottlenecks in the southern lineage that have likely had long-lasting effects on genetic diversity despite an inferred subsequent increase in size, although we emphasize that the population size change patterns for the best-fitting model are likely oversimplistic and likely driven by strong within-lineage population structure in Mexico. Likewise, the migration estimate from the isolation with migration model is also an oversimplification, and recurring migration at the same rate each generation is unlikely, especially given the current distribution of suitable niche-space (Fig. 1), but does indicate the presence of post-divergence gene flow.

The isolated mountain ranges of Mesoamerica have been shown to represent an important biogeographical barrier driving diversification in a number of taxa (Bryson et al. 2011, Ornelas et al. 2013), and existing studies of bumble bees suggest a similar trend. For example, Duennes et al. (2017) demonstrated that the mountain ranges of Mexico produced differing levels of population structure and genetic differentiation within the *Bombus ephippiatus* species complex. Mesoamerica as a whole has been identified as a secondary center of divergence within *Bombus* (Williams et al. 2022). As mentioned above, the Mexico sampling localities demonstrate high levels of differentiation, in line with gaps in suitable habitat outside the mountain ranges where these individuals were collected. This suggests that montane regions of Mexico create a heterogeneous landscape through which gene flow is minimal. Similarly, the signature of population structure and elevated levels of

genetic differentiation between the United States + Canada and Mexico, combined with the lack of suitable habitat connecting these 2 regions, suggests that gene flow is likely minimal or absent in present-day populations, despite early post-divergence gene flow, consistent with the GADMA models. We argue that our results reflect ongoing phylogeographic divergence in *B. huntii*, but that there is currently insufficient evidence for considering multiple species. However, if the spatial availability of suitable niche space remains fragmented and this incipient divergence persists, further diversification from high-elevation isolation is likely, especially in the southern part of the current species range.

Conclusion

Our results support prior results of strong population structure within *B. huntii* and reduced genetic diversity in southern populations compared to northern populations. However, given the recent divergence, potential for post-divergence gene flow, and similarly large population structure among the southern localities, we argue that our results imply that this divergence would not warrant splitting *B. huntii* into different species. Irrespective of species status, localities in the southern part of the *B. huntii* range clearly exhibit substantial isolation and locally strong signals of genome-wide genetic drift, suggesting that the 2 major lineages could be considered as evolutionary significant units. Given increasing interest in developing bumble bee species as domesticated pollinators, it will be important to consider the geographic origins of *B. huntii* colonies if they are deployed for pollination services and to prevent relocation of bees among regions that could erode local genetic diversity (Lozier et al. 2015). Even if rare gene flow does occur, the high levels of genetic differentiation and presence of population structure between northern and southern regions suggest that exchanging individuals between regions has the potential to erode locally adapted alleles. The sampling scheme employed in this study was designed to test the speciation hypothesis and not to detect population-specific local adaptation. But given the population genetic and phylogenomic patterns shown here, future studies incorporating additional samples encompassing a greater representation of the *B. huntii* range will be informative for a better understanding of the population dynamics in this species, especially in Mexico, and for uncovering genomic signatures of natural selection and local adaptation that may better inform sourcing of *B. huntii* for pollination services in different regions.

Specimen Collection Statement

Insect Systematics and Diversity supports compliance with the Nagoya Protocol. The authors attest that all legal and regulatory requirements, including export and import collection permits, have been followed for the collection of specimens from source populations at any international, national, regional, or other geographic level for all relevant field specimens collected as part of this study.

Acknowledgements

USDA ARS provided support to M.G.B. and J.B.K. (project# 2080-30500-001-000D). USDA is an equal opportunity provider and employer. We would like to thank Tien Lindsay for assistance with sample preparation.

Author Contributions

Brandon Austin Meadows (Conceptualization [equal], Data curation [equal], Formal analysis [equal], Investigation [equal], Methodology [equal], Visualization [equal], Writing—original draft [equal], Writing—review & editing [equal]), Jonathan Koch (Conceptualization [equal], Funding acquisition [equal], Investigation [equal], Methodology [equal], Project administration [equal], Resources [equal], Visualization [equal], Writing—review & editing [equal]), Rémy Vandame (Conceptualization [equal], Data curation [equal], Investigation [equal], Resources [equal], Writing—review & editing [equal]), Michael G. Branstetter (Conceptualization [equal], Data curation [equal], Formal analysis [equal], Investigation [equal], Methodology [equal], Validation [equal], Visualization [equal], Writing—original draft [equal], Writing—review & editing [equal]), Ava G. Mckallip (Data curation [equal], Formal analysis [equal], Investigation [equal], Visualization [equal], Writing—original draft [equal]), and Jeffrey Lozier (Conceptualization [equal], Data curation [equal], Formal analysis [equal], Funding acquisition [equal], Investigation [equal], Methodology [equal], Project administration [equal], Resources [equal], Supervision [equal], Validation [equal], Visualization [equal], Writing—original draft [equal], Writing—review & editing [equal])

Supplementary Material

Supplementary material is available at *Insect Systematics and Diversity* online.

Funding

The National Science Foundation provided support to J.D.L. (DEB-2126418), J.B.U.K. (DEB-2126417), and M.G.B. (DEB-2127744). Any opinions, findings, and conclusions or recommendations expressed in this material are those of the authors and do not necessarily reflect the views of the National Science Foundation.

Conflicts of Interest

None declared.

Data Availability

Illumina sequences are available on NCBI SRA accessions SRR30857564-SRR30857602. New DNA barcodes are available in GenBank PP646191- PP646219 (see also Supplementary Data File S1). Variant call files (VCFs), sequence alignments, commands necessary to perform analyses, and important intermediate and results files are available at FigShare (https://doi.org/10.6084/m9.figshare.31956009).

References

Almeida EAB, Bossert S, Danforth BN, et al. 2023. The evolutionary history of bees in time and space. *Curr. Biol.* 33:3409–3422.e6. https://doi.org/10.1016/j.cub.2023.07.005

Bankevich A, Nurk S, Antipov D, et al. 2012. SPAdes: a new genome assembly algorithm and its applications to single-cell sequencing. *J. Comput. Biol.* 19:455–477. https://doi.org/10.1089/cmb.2012.0021

Baur A, Strange JP, Koch JB. 2019. Foraging economics of the hunt bumble bee, a viable pollinator for commercial agriculture. *Environ. Entomol*. 48:799–806. https://doi.org/10.1093/ee/nvz075

Beckham JL, Johnson JA, Pfau RS. 2024. Molecular data support *Bombus sonorus* and *Bombus pensylvanicus* (Hymenoptera, Apidae) as distinct species. *JHR*. 97:895–914. https://doi.org/10.3897/jhr.97.132937

Blaimer BB, Santos BF, Cruaud A, et al. 2023. Key innovations and the diversification of Hymenoptera. *Nat. Commun*. 14:1212. https://doi.org/10.1038/s41467-023-36868-4

Borowiec M. 2019. Spruceup: fast and flexible identification, visualization, and removal of outliers from large multiple sequence alignments. *JOSS*. 4:1635. https://doi.org/10.21105/joss.01635

Borowiec ML. 2016. AMAS: a fast tool for alignment manipulation and computing of summary statistics. *PeerJ* 4:e1660. https://doi.org/10.7717/peerj.1660

Bouckaert R, Vaughan TG, Barido-Sottani J, et al. 2019. BEAST 2.5: an advanced software platform for Bayesian evolutionary analysis. *PLoS Comput. Biol*. 15:e1006650. https://doi.org/10.1371/journal.pcbi.1006650

Branstetter MG, Danforth BN, Pitts JP, et al. 2017a. Phylogenomic insights into the evolution of stinging wasps and the origins of ants and bees. *Curr. Biol*. 27:1019–1025. https://doi.org/10.1016/j.cub.2017.03.027

Branstetter MG, Longino JT, Ward PS, et al. 2017b. Enriching the ant tree of life: enhanced UCE bait set for genome-scale phylogenetics of ants and other Hymenoptera. *Methods Ecol. Evol*. 8:768–776. https://doi.org/10.1111/2041-210X.12742

Bryant D, Bouckaert R, Felsenstein J, et al. 2012. Inferring species trees directly from biallelic genetic markers: bypassing gene trees in a full coalescent analysis. *Mol. Biol. Evol*. 29:1917–1932. https://doi.org/10.1093/molbev/mss086

Bryson RW, Jr., Murphy RW, Lathrop A, et al. 2011. Evolutionary drivers of phylogeographical diversity in the highlands of Mexico: a case study of the *Crotalus triseriatus* species group of montane rattlesnakes. *Journal of Biogeography* 38:697–710. https://doi.org/10.1111/j.1365-2699.2010.02431.x

Button L, Elle E. 2014. Wild bumble bees reduce pollination deficits in a crop mostly visited by managed honey bees. *Agriculture, Ecosystems & Environment* 197:255–263. https://doi.org/10.1016/j.agee.2014.08.004

Cameron SA, Lozier JD, Strange JP, et al. 2011. Patterns of widespread decline in North American bumble bees. *Proc. Natl. Acad. Sci. USA*. 108:662–667. https://doi.org/10.1073/pnas.1014743108

Cameron SA, Sadd BM. 2020. Global trends in bumble bee health. *Annu. Rev. Entomol*. 65:209–232. https://doi.org/10.1146/annurev-ento-011118-111847

Card DC, Shapiro B, Giribet G, et al. 2021. Museum genomics. *Annu. Rev. Genet*. 55:633–659. https://doi.org/10.1146/annurev-genet-071719-020506

Carolan JC, Murray TE, Fitzpatrick Ú, et al. 2012. Colour patterns do not diagnose species: quantitative evaluation of a DNA barcoded cryptic bumblebee complex. *PLoS One*. 7:e29251. https://doi.org/10.1371/journal.pone.0029251

Chambers EA, Lara-Tufiño JD, Campillo-García G, et al. 2025. Distinguishing species boundaries from geographic variation. *Proc. Natl. Acad. Sci. USA* 122:e2423688122. https://doi.org/10.1073/pnas.2423688122

Christmas MJ, Jones JC, Olsson A, et al. 2022. A genomic and morphometric analysis of alpine bumblebees: ongoing reductions in tongue length but no clear genetic component. *Mol. Ecol*. 31:1111–1127. https://doi.org/10.1111/mec.16291

Clement M, Posada D, Crandall KA. 2000. TCS: a computer program to estimate gene genealogies. *Mol. Ecol*. 9:1657–1659. https://doi.org/10.1046/j.1365-294x.2000.01020.x

Cruz CP, Riaño-Jimenez D, Hakim JRC. 2024. Pollination efficiency and foraging behavior of *Bombus pauloensis* (Hymenoptera: Apidae) on two highbush blueberry cultivars (*Vaccinium corymbosum*). *Sociobiology* 71:e9222. https://doi.org/10.13102/sociobiology.v71i1.9222

Danecek P, Auton A, Abecasis G, et al.; 1000 Genomes Project Analysis Group. 2011. The variant call format and VCFtools. *Bioinformatics* 27:2156–2158. https://doi.org/10.1093/bioinformatics/btr330

Danecek P, Bonfield JK, Liddle J, et al. 2021. Twelve years of SAMtools and BCFtools. *Gigascience*. 10:giab008. https://doi.org/10.1093/gigascience/giab008

De Queiroz K. 2007. Species concepts and species delimitation. *Syst. Biol*. 56:879–886. https://doi.org/10.1080/10635150701701083

Duennes MA, Petranek C, de Bonilla EPD, et al. 2017. Population genetics and geometric morphometrics of the *Bombus ephippiatus* species complex with implications for its use as a commercial pollinator. *Conserv. Genet*. 18:553–572. https://doi.org/10.1007/s10592-016-0903-9

Faircloth BC. 2016. PHYLUCE is a software package for the analysis of conserved genomic loci. *Bioinformatics* 32:786–788. https://doi.org/10.1093/bioinformatics/btv646

Folmer O, Black M, Hoeh W, et al. 1994. DNA primers for amplification of mitochondrial cytochrome c oxidase subunit I from diverse metazoan invertebrates. *Mol. Mar. Biol. Biotechnol*. 3:294–299.

Freitas FV, Branstetter MG, Griswold T, et al. 2021. Partitioned gene-tree analyses and gene-based topology testing help resolve incongruence in a phylogenomic study of host-specialist bees (Apidae: Eucerinae). *Mol. Biol. Evol*. 38:1090–1100. https://doi.org/10.1093/molbev/msaa277

Funk DJ, Omland KE. 2003. Species-level paraphyly and polyphyly: frequency, causes, and consequences, with insights from animal mitochondrial DNA. *Annu. Rev. Ecol. Evol. Syst*. 34:397–423. https://doi.org/10.1146/annurev.ecolsys.34.011802.132421

Gain C, François O. 2021. LEA 3: factor models in population genetics and ecological genomics with R. *Mol. Ecol. Resour*. 21:2738–2748. https://doi.org/10.1111/1755-0998.13366

Ghisbain G, Lozier JD, Rahman SR, et al. 2020. Substantial genetic divergence and lack of recent gene flow support cryptic speciation in a colour polymorphic bumble bee (*Bombus bifarius*) species complex. *Syst. Entomol*. 45:635–652. https://doi.org/10.1111/syen.12419

Glück M, Geue JC, Thomassen HA. 2022. Environmental differences explain subtle yet detectable genetic structure in a widespread pollinator. *BMC Ecol. Evol*. 22:8. https://doi.org/10.1186/s12862-022-01963-5

Gmel AI, Guichard M, Dainat B, et al.; Beestrong Consortium. 2023. Identification of runs of homozygosity in Western honey bees (*Apis mellifera*) using whole-genome sequencing data. *Ecol. Evol*. 13:e9723. https://doi.org/10.1002/ece3.9723

Gornall L, Dauber J, Sickel W. 2025. Population delimitation in bumble bees—strategies and research gaps. *Front. Bee Sci*. 3:1507903. https://doi.org/10.3389/frbee.2025.1507903

Gruber B, Unmack PJ, Berry OF, et al. 2018. dartr: an R package to facilitate analysis of SNP data generated from reduced representation genome sequencing. *Mol. Ecol. Resour*. 18:691–699. https://doi.org/10.1111/1755-0998.12745

Guindon S, Dufayard J-F, Lefort V, et al. 2010. New algorithms and methods to estimate maximum-likelihood phylogenies: assessing the performance of PhyML 3.0. *Syst. Biol*. 59:307–321. https://doi.org/10.1093/sysbio/syq010

Gutenkunst RN, Hernandez RD, Williamson SH, et al. 2009. Inferring the joint demographic history of multiple populations from multidimensional SNP frequency data. *PLoS Genet*. 5:e1000695. https://doi.org/10.1371/journal.pgen.1000695

Hebert PDN, Ratnasingham S, de Waard JR. 2003. Barcoding animal life: cytochrome c oxidase subunit 1 divergences among closely related species. *Proc. R Soc. Lond. B* 270:S96–S99. https://doi.org/10.1098/rsbl.2003.0025

Heraghty SD, Jackson JM, Lozier JD. 2023. Whole genome analyses reveal weak signatures of population structure and environmentally associated local adaptation in an important North American pollinator, the bumble bee *Bombus vosnesenskii*. *Mol. Ecol*. 32:5479–5497. https://doi.org/10.1111/mec.17125

Heraghty SD, Rahman SR, Jackson JM, et al. 2022. Whole genome sequencing reveals the structure of environment-associated divergence in a broadly distributed montane bumble bee, *Bombus vancouverensis*. *Insect Systematics and Diversity* 6:5. https://doi.org/10.1093/isd/ixac025

Hines HM. 2008. Historical biogeography, divergence times, and diversification patterns of bumble bees (Hymenoptera: Apidae: Bombus). *Syst. Biol.* 57:58–75. https://doi.org/10.1080/10635150801898912

Hines HM, Cameron SA, Williams PH. 2006. Molecular phylogeny of the bumble bee subgenus Pyrobombus (Hymenoptera: Apidae : Bombus) with insights into gene utility for lower-level analysis. *Invertebrate Systematics* 20:289–303. https://doi.org/10.1071/IS05028

Hoang DT, Chernomor O, Von Haeseler A, et al. 2018. UFBoot2: improving the ultrafast bootstrap approximation. *Mol. Biol. Evol.* 35:518–522. https://doi.org/10.1093/molbev/msx281

Jackson JM, Pimsler ML, Oyen KJ, et al. 2018. Distance, elevation and environment as drivers of diversity and divergence in bumble bees across latitude and altitude. *Mol. Ecol.* 27:2926–2942. https://doi.org/10.1111/mec.14735

Jha S. 2015. Contemporary human-altered landscapes and oceanic barriers reduce bumble bee gene flow. *Mol. Ecol.* 24:993–1006. https://doi.org/10.1111/mec.13090

Jombart T, Ahmed I. 2011. *adegenet 1.3-1*: new tools for the analysis of genome-wide SNP data. *Bioinformatics* 27:3070–3071. https://doi.org/10.1093/bioinformatics/btr521

Jouganous J, Long W, Ragsdale AP, et al. 2017. Inferring the joint demographic history of multiple populations: beyond the diffusion approximation. *Genetics* 206:1549–1567. https://doi.org/10.1534/genetics.117.200493

Kalyaanamoorthy S, Minh BQ, Wong TK, et al. 2017. ModelFinder: fast model selection for accurate phylogenetic estimates. *Nat. Methods*. 14:587–589. https://doi.org/10.1038/nmeth.4285

Kardos M, Waples RS. 2025. Low-coverage sequencing and Wahlund effect severely bias estimates of inbreeding, heterozygosity and effective population size in North American wolves. *Mol. Ecol.* 34:e17415. https://doi.org/10.1111/mec.17415

Knaus BJ, Grünwald NJ. 2017. VCFR: a package to manipulate and visualize variant call format data in R. *Mol. Ecol. Resour*. 17:44–53. https://doi.org/10.1111/1755-0998.12549

Koch J, Strange J, Williams PH. (2012). Bumble bees of the western United States. U.S. Department of Agriculture, Forest Service.

Koch JB, Vandame R, Mérida-Rivas J, et al. 2018. Quaternary climate instability is correlated with patterns of population genetic variability in *Bombus huntii*. *Ecol. Evol.* 8:7849–7864. https://doi.org/10.1002/ece3.4294

Koch JBU, Sim SB, Scheffler B, et al. 2024. Chromosome-scale genome assembly of the hunt bumble bee, *Bombus huntii* Greene, 1860, a species of agricultural interest. *G3 (Bethesda)* 14:jkae160. https://doi.org/10.1093/g3journal/jkae160

Korunes KL, Samuk K. 2021. pixy: unbiased estimation of nucleotide diversity and divergence in the presence of missing data. *Mol. Ecol. Resour*. 21:1359–1368. https://doi.org/10.1111/1755-0998.13326

Leigh JW, Bryant D. 2015. POPART: full-feature software for haplotype network construction. *Methods Ecol. Evol.* 6:1110–1116. https://doi.org/10.1111/2041-210X.12410

Li H. 2013. Aligning sequence reads, clone sequences and assembly contigs with BWA-MEM (arXiv:1303.3997). ArXiv. https://doi.org/10.48550/arXiv.1303.3997, preprint: not peer reviewed.

Li H, Handsaker B, Wysoker A, et al.; 1000 Genome Project Data Processing Subgroup. 2009. The sequence alignment/map format and SAMtools. *Bioinformatics* 25:2078–2079. https://doi.org/10.1093/bioinformatics/btp352

Liu H, Jia Y, Sun X, et al. 2017. Direct determination of the mutation rate in the Bumblebee reveals evidence for weak recombination-associated mutation and an approximate rate constancy in insects. *Mol. Biol. Evol.* 34:119–130. https://doi.org/10.1093/molbev/msw226

Lozier JD. 2014. Revisiting comparisons of genetic diversity in stable and declining species: assessing genome-wide polymorphism in North American bumble bees using RAD sequencing. *Mol. Ecol.* 23:788–801. https://doi.org/10.1111/mec.12636

Lozier JD, Cameron SA, Duennes MA, et al. 2015. Relocation risky for bumblebee colonies. *Science* 350:286–287. https://doi.org/10.1126/science.350.6258.286-b

Lozier JD, Ols CN, Pitsenberger CA, et al. 2020. Partitioning of bee diversity at a small spatial scale in an urban arboretum. *Southeastern Nat.* 19:22. https://doi.org/10.1656/058.019.0103

Lozier JD, Strange JP, Heraghty SD. 2023. Whole genome demographic models indicate divergent effective population size histories shape contemporary genetic diversity gradients in a montane bumble bee. *Ecol. Evol.* 13:e9778. https://doi.org/10.1002/ece3.9778

Maddison WP. 1997. Gene trees in species trees. *Syst. Biol.* 46:523–536. https://doi.org/10.1093/sysbio/46.3.523

Martin M. 2011. Cutadapt removes adapter sequences from high-throughput sequencing reads. *EMBnet J.* 17:10–12. https://doi.org/10.14806/ej.17.1.200

McKenna A, Hanna M, Banks E, et al. 2010. The Genome Analysis Toolkit: a MapReduce framework for analyzing next-generation DNA sequencing data. *Genome Res.* 20:1297–1303. https://doi.org/10.1101/gr.107524.110

Minh BQ, Nguyen MAT, Von Haeseler A. 2013. Ultrafast approximation for phylogenetic bootstrap. *Mol. Biol. Evol.* 30:1188–1195. https://doi.org/10.1093/molbev/mst024

Minh BQ, Schmidt HA, Chernomor O, et al. 2020. IQ-TREE 2: new models and efficient methods for phylogenetic inference in the genomic era. *Mol. Biol. Evol.* 37:1530–1534. https://doi.org/10.1093/molbev/msaa015

Mola JM, Pearse IS, Boone ML, et al. 2024. Range-wide genetic analysis of an endangered bumble bee (*Bombus affinis*, Hymenoptera: Apidae) reveals population structure, isolation by distance, and low colony abundance. *J. Insect Sci.* 24:19. https://doi.org/10.1093/jisesa/ieae041

Noskova E, Abramov N, Iliutkin S, et al. 2022. GADMA2: more efficient and flexible demographic inference from genetic data. *Gigascience*. 12:giad059. https://doi.org/10.1093/gigascience/giad059

Ornelas JF, Sosa V, Soltis DE, et al. 2013. Comparative phylogeographic analyses illustrate the complex evolutionary history of threatened cloud forests of northern Mesoamerica. *PLoS One*. 8:e56283. https://doi.org/10.1371/journal.pone.0056283

Ortiz EM. 2019. vcf2phylip v2.0: convert a VCF matrix into several matrix formats for phylogenetic analysis. Version v2. [Computer software]. *Zenodo*. https://doi.org/10.5281/ZENODO.2540861

Purcell S, Neale B, Todd-Brown K, et al. 2007. PLINK: a tool set for whole-genome association and population-based linkage analyses. *Am. J. Hum. Genet.* 81:559–575. https://doi.org/10.1086/519795

Rambaut A. (2018). FigTree v1.4.4: tree figure drawing tool. Version 1.4.4. [Computer software]. http://tree.bio.ed.ac.uk/software/figtree/

Rambaut A, Drummond AJ, Xie D, et al. 2018. Posterior summarization in Bayesian phylogenetics using Tracer 1.7. *Syst. Biol.* 67:901–904. https://doi.org/10.1093/sysbio/syy032

Robinson JA, Kyriazis CC, Nigenda-Morales SF, et al. 2022. The critically endangered vaquita is not doomed to extinction by inbreeding depression. *Science* 376:635–639. https://doi.org/10.1126/science.abm1742

Rohde AT, Strange JP, Tobin KB, et al. 2025. Genome-wide markers test the status of two putative species of North American bumble bees. *Conserv. Genet.* 26:429–448. https://doi.org/10.1007/s10592-025-01674-6

Sakulich EM, Koch JBU, Strange JP. 2025. Population structure varies among 4 western North American bumble bee species. *Insect Systematics and Diversity* 9:4. https://doi.org/10.1093/isd/ixaf003

Sang H, Li Y, Tan S, et al. 2024. Conservation genomics analysis reveals recent population decline and possible causes in bumblebee *Bombus opulentus*. *Insect Sci.* 31:1631–1644. https://doi.org/10.1111/1744-7917.13324

Santos Júnior JE, Williams PH, Dias CAR, et al. 2022. Biogeography and diversification of bumblebees (Hymenoptera: Apidae), with emphasis on neotropical species. *Diversity* (*Basel)* 14:238. https://doi.org/10.3390/d14040238

Schweizer RM, Grummer JA, Tobin KB, et al. 2025. Museum genomics suggests long-term population decline in a putatively extinct bumble bee. *Proc. Natl. Acad. Sci. USA*. 122:e2509749122. https://doi.org/10.1073/pnas.2509749122

Sheffield CS, Richardson L, Cannings S, et al. 2016. Biogeography and designatable units of *Bombus occidentalis* Greene and *B. terricola* Kirby (Hymenoptera: Apidae) with implications for conservation status assessments. *J. Insect Conserv*. 20:189–199. https://doi.org/10.1007/s10841-016-9853-2

Sousa PD, Henriques A, Silva SE, et al. 2023. Genomic patterns of Iberian wild bees reveal levels of diversity, differentiation and population structure, supporting the "refugia within refugia" hypothesis. *Diversity* (*Basel)* 15:746. https://doi.org/10.3390/d15060746

Sproul JS, Maddison DR. 2017. Sequencing historical specimens: successful preparation of small specimens with low amounts of degraded DNA. *Mol. Ecol. Resour*. 17:1183–1201. https://doi.org/10.1111/1755-0998.12660

Stange M, Sánchez-Villagra MR, Salzburger W, et al. 2018. Bayesian divergence-time estimation with genome-wide single-nucleotide polymorphism data of sea catfishes (Ariidae) supports Miocene closure of the Panamanian Isthmus. *Syst. Biol*. 67:681–699. https://doi.org/10.1093/sysbio/syy006

Stoltz M, Baeumer B, Bouckaert R, et al. 2021. Bayesian inference of species trees using diffusion models. *Syst. Biol*. 70:145–161. https://doi.org/10.1093/sysbio/syaa051

Strange JP. 2015. *Bombus huntii*, *Bombus impatiens*, and *Bombus vosnesenskii* (Hymenoptera: Apidae) pollinate greenhouse-grown tomatoes in western North America. *J. Econ. Entomol*. 108:873–879. https://doi.org/10.1093/jee/tov078

Strange J, Colla S, Davies Adams L, et al. 2023. An evidence-based rationale for a North American commercial bumble bee clean stock certification program. *J. Pollinat. Ecol*. 33:1–13. https://doi.org/10.26786/1920-7603(2023)721

Tagliacollo VA, Lanfear R. 2018. Estimating improved partitioning schemes for ultraconserved elements. *Mol. Biol. Evol*. 35:1798–1811. https://doi.org/10.1093/molbev/msy069

Talavera G, Castresana J. 2007. Improvement of phylogenies after removing divergent and ambiguously aligned blocks from protein sequence alignments. *Syst. Biol*. 56:564–577. https://doi.org/10.1080/10635150701472164

Velthuis HHW, Van Doorn A. 2006. A century of advances in bumblebee domestication and the economic and environmental aspects of its commercialization for pollination. *Apidologie* 37:421–451. https://doi.org/10.1051/apido:2006019

Weir BS, Cockerham CC. 1984. Estimating F-statistics for the analysis of population structure. *Evolution* 38:1358–1370. https://doi.org/10.2307/2408641

Wickham H. 2011. Ggplot2. *WIREs Comput. Stats*. 3:180–185. https://doi.org/10.1002/wics.147

Williams PH. (1998). An annotated checklist of bumble bees with an analysis of patterns of description (Hymenoptera: Apidae, Bombini). *Bull. Nat. Hist. Mus*. 69:79–152. https://biostor.org/reference/111695

Williams PH. 2021. Not just cryptic, but a barcode bush: PTP re-analysis of global data for the bumblebee subgenus *Bombus s. str*. supports additional species (Apidae, genus *Bombus*). *J. Nat. Hist*. 55:271–282. https://doi.org/10.1080/00222933.2021.1900444

Williams PH. 2022. Novel splitting/lumping index reflects the history of species concepts applied to bumblebees (Insecta: Apidae). *Zoological Journal of the Linnean Society* 196:704–719. https://doi.org/10.1093/zoolinnean/zlab123

Williams PH, Cannings SG, Sheffield CS. 2016. Cryptic subarctic diversity: a new bumblebee species from the Yukon and Alaska (Hymenoptera: Apidae). *J. Nat. Hist*. 50:2881–2893. https://doi.org/10.1080/00222933.2016.1214294

Williams PH, Dorji P, Ren Z, et al. 2022. Bumblebees of the hypnorum-complex world-wide including two new near-cryptic species (Hymenoptera: Apidae). *EJT*. 847. https://doi.org/10.5852/ejt.2022.847.1981

Williams PH, Françoso E, Martinet B, et al. 2022. When did bumblebees reach South America? Unexpectedly old montane species may be explained by Mexican stopover (Hymenoptera: Apidae). *Syst. Biodivers*. 20:1–24. https://doi.org/10.1080/14772000.2022.2092229

Wingett SW, Andrews S. 2018. FastQ Screen: a tool for multi-genome mapping and quality control. *F1000Res*. 7:1338. https://doi.org/10.12688/f1000research.15931.2

Wutke S, Blank SM, Boevé J-L, et al. 2024. Phylogenomics and biogeography of sawflies and woodwasps (Hymenoptera, Symphyta). *Mol. Phylogenet. Evol*. 199:108144. https://doi.org/10.1016/j.ympev.2024.108144

Yeates DK, Zwick A, Mikheyev AS. 2016. Museums are biobanks: unlocking the genetic potential of the three billion specimens in the world's biological collections. *Curr. Opin. Insect Sci*. 18:83–88. https://doi.org/10.1016/j.cois.2016.09.009

Zarn KE, Roffler GH, Kardos M, et al. 2025. Genomic analysis reveals inbreeding in an island population of Alexander Archipelago wolves. *Evol. Appl*. 18:e70144. https://doi.org/10.1111/eva.70144

Zimmerman SJ, Aldridge CL, Oyler-McCance SJ. 2020. An empirical comparison of population genetic analyses using microsatellite and SNP data for a species of conservation concern. *BMC Genomics*. 21:382. https://doi.org/10.1186/s12864-020-06783-9

Published by Oxford University Press on behalf of Entomological Society of America 2026.
This work is written by (a) US Government employee(s) and is in the public domain in the US. Insect Systematics and Diversity 2026 10(5) 1–17
https://doi.org/10.1093/isd/ixag040
Research Evolution